Remote Sensing of Environment 129 (2013) 210–230

Contents lists available at SciVerse ScienceDirect

Remote Sensing of Environment

journal homepage: www.elsevier.com/locate/rse

Spectroscopic remote sensing of the distribution and persistence of oil from the Deepwater Horizon spill in Barataria Bay marshes

Raymond F. Kokaly [a,*], Brady R. Couvillion [b], JoAnn M. Holloway [a], Dar A. Roberts [c], Susan L. Ustin [d], Seth H. Peterson [c], Shruti Khanna [d], Sarai C. Piazza [b]

[a] U.S. Geological Survey, MS 973, Box 25046, Denver Federal Center, Denver, CO 80225, USA
[b] U.S. Geological Survey, C/O Livestock Show Office, Parker Coliseum, Baton Rouge, LA 70803, USA
[c] Geography Department, University of California, Santa Barbara, Santa Barbara, CA 93106, USA
[d] Department of Land, Air, and Water Resources, University of California, Davis, Davis, CA 95616, USA

ARTICLE INFO

Article history:
Received 27 March 2012
Received in revised form 10 October 2012
Accepted 11 October 2012
Available online 5 December 2012

Keywords:
Hyperspectral
Ecosystem disturbance and response
Imaging spectroscopy
Hydrocarbon
Oil spill
Coastal wetlands

ABSTRACT

We applied a spectroscopic analysis to Airborne Visible/InfraRed Imaging Spectrometer (AVIRIS) data collected from low and medium altitudes during and after the Deepwater Horizon oil spill to delineate the distribution of oil-damaged canopies in the marshes of Barataria Bay, Louisiana. Spectral feature analysis compared the AVIRIS data to reference spectra of oiled marsh by using absorption features centered near 1.7 and 2.3 μm, which arise from C–H bonds in oil. AVIRIS-derived maps of oiled shorelines from the individual dates of July 31, September 14, and October 4, 2010, were 89.3%, 89.8%, and 90.6% accurate, respectively. A composite map at 3.5 m grid spacing, accumulated from the three dates, was 93.4% accurate in detecting oiled shorelines. The composite map had 100% accuracy for detecting damaged plant canopy in oiled areas that extended more than 1.2 m into the marsh. Spatial resampling of the AVIRIS data to 30 m reduced the accuracy to 73.6% overall. However, detection accuracy remained high for oiled canopies that extended more than 4 m into the marsh (23 of 28 field reference points with oil were detected). Spectral resampling of the 3.5 m AVIRIS data to Landsat Enhanced Thematic Mapper (ETM) spectral response greatly reduced the detection of oil spectral signatures. With spatial resampling of simulated Landsat ETM data to 30 m, oil signatures were not detected. Overall, ~40 km of coastline, marsh comprised mainly of *Spartina alterniflora* and *Juncus roemerianus*, were found to be oiled in narrow zones at the shorelines. Zones of oiled canopies reached on average 11 m into the marsh, with a maximum reach of 21 m. The field and airborne data showed that, in many areas, weathered oil persisted in the marsh from the first field survey, July 10, to the latest airborne survey, October 4, 2010. The results demonstrate the applicability of high spatial resolution imaging spectrometer data to identifying contaminants in the environment for use in evaluating ecosystem disturbance and response.

Published by Elsevier Inc.

1. Introduction

The marsh ecosystems of southern Louisiana have been subject to degradation and erosion at high rates leading to a net decrease in wetland area of over 4800 km^2 in the last 78 years (Couvillion et al., 2011; Day et al., 2005). Among the many factors contributing to this land loss is anthropogenic pollution including hydrocarbons released in near-shore oil spills (Borja et al., 2010). Physical and chemical effects of oil spills can have both short- and long-term impacts on wetland function, including the interruption of benthic biogeochemical processes and decreased primary production (Carman et al., 1997; Catallo, 1993; Lin & Mendelssohn, 1996; Pezeshki et al., 2000). Oil contamination can lead to plant mortality, loss of habitat integrity, and an increased susceptibility to marsh collapse (Ko & Day, 2004; Lin & Mendelssohn, 2009).

On the evening of April 20, 2010, an explosion occurred on the Deepwater Horizon drilling unit approximately 64 km off the Louisiana coast (National Committee on the BP Deepwater Horizon Oil Spill and Offshore Drilling, 2011). Oil leaked until a capping stack was installed on July 15; in that time period, 4.4 million barrels of oil leaked from the Macondo well (Crone & Tolstoy, 2010). During the Deepwater Horizon incident, researchers at the U.S. Geological Survey (USGS), National Aeronautics and Space Administration (NASA), National Oceanic and Atmospheric Administration (NOAA) and academic institutions cooperatively organized flights of advanced remote sensing instruments to assist in the coordinated response to the oil spill. As part of that response, data were collected using NASA's Airborne Visible/InfraRed Imaging Spectrometer (AVIRIS; Green et al., 1998) from early May to early October in order to detect and quantify thick oil emulsions on the ocean's surface (Clark et al., 2010; Kokaly et

* Corresponding author. Tel.: +1 303 236 1359.
E-mail address: raymond@usgs.gov (R.F. Kokaly).

0034-4257/$ – see front matter. Published by Elsevier Inc.
http://dx.doi.org/10.1016/j.rse.2012.10.028

al., 2010) and characterize the extent of oil impacts on marsh ecosystems.

Recent studies have indicated the potential for using remote sensing to characterize oil contamination on the ocean's surface by using spectroscopy (Lammoglia & Souza Filho, 2011) and broad-band multispectral data (Lammoglia & Souza Filho, 2012). Past laboratory and field studies have indicated the potential for using imaging spectrometer data for detecting oil contamination on land (Kühn et al., 2004). The hydrocarbon index (HI) of Kühn et al. (2004) is focused on a single absorption feature in the radiance data measured by imaging spectrometers. Background materials with overlapping absorption features, such as dry vegetation, can have high HI values similar to hydrocarbons.

The practical, widespread application of imaging spectrometers to detect oil contamination in the natural environment has the potential to complement the application of this same technology to evaluating ecosystem response to oil disturbance. Many studies have found imaging spectroscopy to be useful for characterizing ecosystem disturbances and for studying the post-disturbance landscape (Asner & Vitousek, 2005; Dennison et al., 2006; Kokaly et al., 2003, 2007, 2007; Li et al., 2005; Riaño et al., 2002). AVIRIS data of the oil-impacted coasts complement coarser spatial resolution multispectral data from Landsat (Mishra et al., 2012) and radar backscatter data from UAVSAR (Ramsey et al., 2011). The power of a spectroscopic method for identifying a specific material in data from a single date of collection is a unique contribution compared to approaches reliant on inferred differences in pre- and post-impact imagery.

In this work, we developed a spectroscopic approach to detect oil. We applied this method to AVIRIS data collected over the marshes in southern Louisiana. The key aspect of the detection method is a spectral feature analysis of two hydrocarbon absorption features, centered near 1.72 and 2.3 μm, which arise from the C – H bonds in oil (Cloutis, 1989). This oil detection method was applied to AVIRIS coverage of the heavily oiled Barataria Bay area obtained on July 31, September 14, and October 4, 2010. Map accuracy was assessed using field observations on oiling. Map evaluation was also conducted for results obtained after spatial resampling of the AVIRIS data from 3.5 to 30 m and the spectral resampling of the AVIRIS data to Landsat ETM.

2. Material and methods

2.1. Field surveys and the Barataria Bay study area

Field work was conducted in southern Louisiana in June, July, and August, 2010. An initial visit was made on June 7–8, 2010, to measure the reflectance spectra of marsh plants in areas that were at potential risk of oiling in conjunction with routine vegetation survey work at sites of the Coastal Reference Monitoring System (CRMS; Steyer et al., 2003). Vegetation cover by species was quantified for ten 2×2 m subplots at each of three CRMS sites. The sites surveyed included CRMS0121 in Bayou Long at 29.6938° N, 89.823° W (see Fig. 1). Also surveyed in June were CRMS0322 and CRMS0326 situated east of Terrebonne Bay at 29.2438° N, 91.1045° W and 29.2728° N, 91.073° W, respectively. On June 9, 2010, field work was conducted on Grand Isle, Louisiana (see Fig. 1), in order to measure the reflectance spectra of oil that had made landfall on the sand beaches of this barrier island. Measurements of reflectance are described in Sections 2.2 and 2.6 below.

Based on initial information on oiled shorelines available during the spill from operational response teams using Shoreline Cleanup Assessment Techniques (SCAT, 2012), Barataria Bay and the Bird's Foot Delta of the Mississippi River (see Fig. 1) were selected for survey in July, 2010, in order to measure reflectance spectra of a variety of marsh plant species in areas of oiling and to document conditions of oiling and oil impact on plant canopies. On July 8, field spectra of oiled vegetation, non-oiled vegetation, and other materials were measured in the Bird's Foot Delta. On July 10, the field spectra were collected in northern Barataria Bay. Locations of survey points were selected based on access to the marsh through gaps in protective booms. At each survey point, descriptions of vegetation species composition and canopy condition, presence of oil, and oil impacts on plants and sediment were recorded. In addition, measurements were made on the lateral distance of oil penetration into the marsh and the linear extent of oil along the shore by using a tape measure (meter scale) or a laser rangefinder (Nikon ProStaff).

Repeat surveys of the Barataria Bay and the Bird's Foot Delta areas were made in August for field reflectance measurements and to continue documenting conditions of oiling and oil impact on plant canopies. The Bird's Foot Delta was revisited on August 14, 2010. Barataria Bay was surveyed again on August 12–13, 2010. During the August 12–14 survey, areas of extensive oiling detected in the preliminary analyses of July 31 AVIRIS data guided the point locations. However, sampling locations were again limited to gaps in protective booms.

Because of the greater extent of oiling observed in field surveys, Barataria Bay was selected for continued field work and as the focal area of this study (Fig. 1). In particular, the Bay Jimmy subarea of Barataria Bay was the location of most field work (see section Fig. 1). Barataria Basin encompasses an area of approximately 5720 km^2 of open water and wetland areas with vegetation ranging from forested wetlands in the upper basin to saline marshes in the lower portions which include the Bay Jimmy subarea. The emergent marsh vegetation is typical of a saline community and is dominated by *S. alterniflora*, *J. roemerianus*, and *Distichlis spicata*. During the study period, surface water salinity averaged 3.07 ± 1.6 as measured at 5 CRMS sites near the study area. Soils in this region are comprised of sedimentary materials sourced from fluvial and tidally redistributed deposits (Louisiana Office of Coastal Protection and Restoration, 2012). In the lower Barataria Basin, diurnal spring tidal ranges are approximately 50 cm (Snedden, 2006). The major water exchange mechanisms between the Gulf of Mexico and the Barataria Basin include tides, wind driven winter storms (occurring every 4 to 7 days (Chuang & Wiseman, 1983)), and tropical events. Tropical storm events do not occur frequently but account for large water exchanges between the estuary and the coastal ocean while causing pronounced flooding of the marsh platform with saline waters. One tropical depression made landfall within Louisiana waters during the study period (Bonnie, July 22–24, 2010; National Oceanic and Atmospheric Administration, National Weather Service, National Hurricane Center. http://www.nhc.noaa.gov/2010atlan.shtml).

Altered hydrology, sediment deprivation, oil and gas activities, and other natural and anthropogenic factors have contributed to a rapid land change in this area. The Barataria Basin accounts for approximately 25% of the total wetland loss experienced in coastal Louisiana from 1932 to 2010 (Couvillion et al., 2011). The overwhelming majority of this loss has occurred in the lower portions of the basin which include Bay Jimmy.

A final field survey in 2010 was conducted to revisit sites and access heavily oiled areas that could not be reached in the mid-August survey. Field observations made during the July and August surveys were summarized by Kokaly et al. (2011). In addition to characterizing marsh conditions and degree of oiling, dissolved organic carbon (DOC) concentrations in water samples were collected from two open-water sites and from the soil/water interface (1–3 cm of standing water in contact with soil surface) in the Barataria Bay marshes on August 24–26, 2010. Water sampling and DOC analysis were conducted to determine the extent to which hydrocarbons were partitioned into the dissolved fraction, which could potentially enhance plant regrowth in oil-impacted zones. Water samples were collected by peristaltic pump in line with a 0.2 μm polycarbonate filter from standing water roughly within 2 cm of the soil–water interface in marshes. Samples for dissolved organic carbon (DOC) were collected into amber glass vials pre-cleaned for organic compounds. Open water samples were collected at two sites. These samples were taken as grab samples into

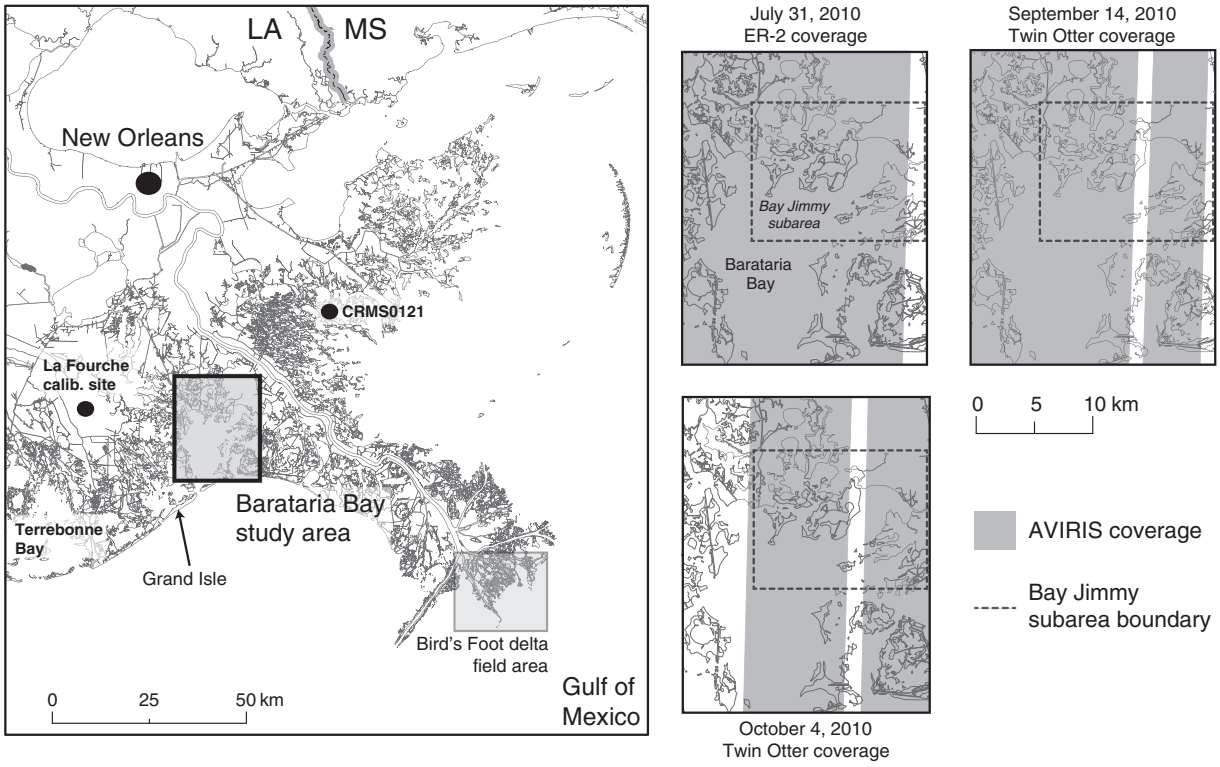

Fig. 1. Location of the Barataria Bay study area and coverage by AVIRIS. The Bay Jimmy subarea is marked on the July 31, September 14, and October 4, 2010, coverage maps. Shoreline is the NOAA Medium Resolution Digital Vector Shoreline.
Available from http://www.ngdc.noaa.gov/mgg/shorelines/noaamrdvs.html.

pre-cleaned amber glass holding bottles. Samples were filtered from the holding bottles into sample containers within 30 min of collection. Samples were chilled in the field to 4 °C and were maintained at that temperature until analysis. DOC was analyzed following the Pt catalyzed persulfate wet oxidation method (Aiken, 1992).

2.2. Reference spectral library of oiled and non-oiled materials

The Material Identification and Characterization Algorithm (MICA), a module of the USGS Processing Routines in IDL for Spectroscopic Measurements (PRISM; Kokaly, 2011) software, was used to compare the spectrum of each pixel of the AVIRIS data to reference spectra of oil, oiled marsh, and non-oiled vegetation. Five reference spectra of oiled plants and marsh, one reference spectrum of oil, and three reference spectra of non-oiled vegetation were included in the reference spectral library (Fig. 2). The reference spectra, absorption features and descriptions of the materials measured are given in Table 1. Because of persistent cloud cover and restricted access to oiled shorelines caused by the placement of protective booms, measurements of oiled areas were difficult to obtain using reflected sunlight. Therefore, three samples of oiled vegetation were collected and subsequently measured using an Analytical Spectral Devices (ASD) FieldSpec 3 (FS3) spectrometer, covering the wavelength range of 0.35 to 2.5 μm, with an artificial light source in the laboratory (see the spectra labeled Oiled-Plants1, Oiled-Plants2, and Oiled-Plants3 in Fig. 2 and Table 1). All ASD spectra used in this study were collected with the spectrometer set to average 60 samples per recording, with 240 samples averaged in the white reference and dark current measurements. A Spectralon panel was used as the white reference material. One sample of oiled *Phragmites australis* was collected on July 8 and two samples of oiled *S. alterniflora* mixed with *J. roemerianus* were collected on July 10. These samples were placed on ice to prevent degradation and stored until their reflectance spectra were measured on July 11.

On August 13, 2010, two areas of oiled marsh were measured in the sunlight using the ASD FS3 with bare fiber held at approximately 1.33 m height above the oiled canopy with nadir pointing (see the spectra labeled Oiled-Marsh and Oiled-Dry-Marsh in Fig. 2 and Table 1). On June 9, 2010, an area of black, pooled oil (1 m^2) on the beach at Grand Isle, Louisiana, was measured in sunlight (see the spectrum labeled Oil-strong in Fig. 2 and Table 1). The oiled plant, oiled marsh, and pooled oil spectra are collectively referred to as reference spectra of oiled materials. These spectra show varying strengths of absorption features at 1.72 and 2.3 μm, which are features arising from C–H bonds in the oil (Cloutis, 1989).

Non-oiled, dry, non-photosynthetic vegetation (NPV) materials were included as reference spectra because of the similar wavelength positions of absorption features caused by leaf biochemical constituents such as cellulose and lignin (Elvidge, 1990). The spectra of dry, brown leaves and stems of *S. alterniflora* were measured in the field using the ASD FS3 with a contact probe (an artificial light source) on June 7, 2010 (see the spectrum labeled Veg-DrySpartina in Fig. 2 and Table 1). The spectra of dry, brown leaves of *P. australis* were measured using the ASD FS3 with a contact probe on July 8, 2010 (see the spectrum labeled Veg-DryPhragmites in Fig. 2 and Table 1). The ASD contact probe is an artificial light source with a restricted, 1 cm diameter, field of view. To measure reflectance using the contact probe, plant stems and leaves in the top 30 cm of the canopy were bunched together. The contact probe was pressed against the optically thick bundle and a spectrum was recorded at two positions along the length of the bundle. For *S. alterniflora* and *P. australis*, nine bundles for each were measured for subsequent averaging.

From the USGS Spectral Library version 6 (Clark et al., 2007), an existing vegetation spectrum with a deep chlorophyll absorption was used as a reference spectrum (see the spectrum labeled Veg-StrongChlorophyll in Fig. 2 and Table 1). All ASD spectra used in this study were corrected for detector offsets and converted to absolute

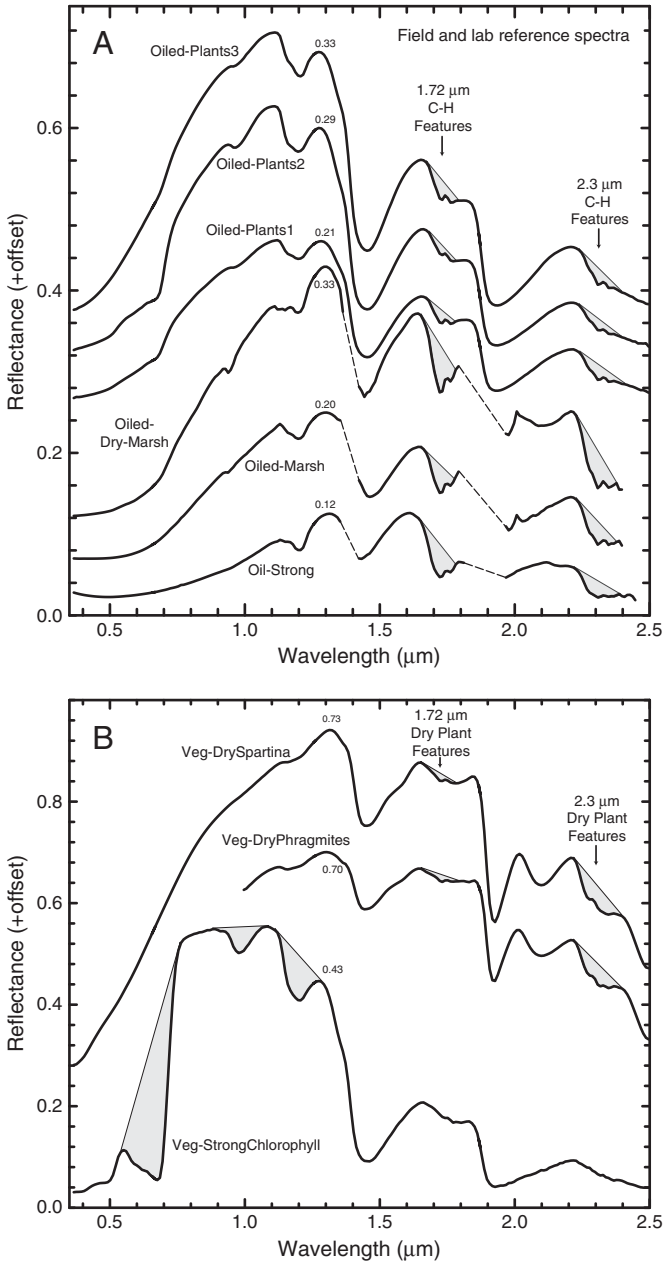

Fig. 2. A) Reference spectra of oiled plants, oiled marsh, and pooled oil. The spectra are offset for clarity; the additive offset factors are 0, 0.05, 0.10, 0.25, 0.30, and 0.35 for the spectra from bottom to top. B) Reference spectra of non-oiled vegetation. The spectra are offset for clarity; the additive offset factors are 0, 0, and 0.20 for the spectra from bottom to top. The samples and survey sites describing the material that was measured are listed in Table 1. Continuum lines used to define the absorption features that were analyzed to detect these materials are shown with a thin line and the corresponding areas of the absorption features are shaded in light gray. Channels in wavelength regions of strong atmospheric absorption were deleted from field spectra measured with sunlight as the illumination. These regions in the spectra are shown by a thin, dashed line.

reflectance (Kokaly, 2011). In addition, all spectra were convolved (Kokaly, 2011) from their original spectrometer wavelength sampling and bandpass characteristics to the AVIRIS sensor characteristics before comparison to or use in processing AVIRIS data.

2.3. AVIRIS data, reflectance conversion, and geocorrection

The processing flow for each single date of the AVIRIS data, from radiance data to a map of oiling, is shown in Fig. 3. The details of the processing steps are described in this and subsequent subsections. The AVIRIS data over the study area were collected from the NASA ER-2 aircraft, at an altitude of 9.1 km on July 31, and from a Twin Otter aircraft, at an altitude of 4.1 km on September 14 and October 4 (see Fig. 1). The AVIRIS radiance data were atmospherically corrected and converted to apparent surface reflectance using mode 1.5 of the ACORN (Atmospheric CORrection Now) radiative transfer correction program (ImSpec LLC, Palmdale, CA).

On June 27, 2010, field spectrometer measurements were made using an ASD Field Spec Pro spectrometer (Analytical Spectral Devices, Boulder, CO) of a single ground calibration site. The calibration site was an airport parking ramp with approximate dimensions of 90 m north to south and 30 m east to west, located at the La Fourche airport, 29° 26′ 37′ N latitude and 90° 15′ 47′ W longitude, approximately 20 km west of Barataria Bay (see Fig. 1). Field-measured reflectance of the calibration site was used to remove residual atmospheric absorption features to produce radiative-transfer-ground-calibrated (RTGC) reflectance data (Clark et al., 2002). The ground calibration site was covered by an AVIRIS flight line on each date of collection. Multiplicative correction factors for each channel of the AVIRIS data were generated for each flight day to remove the residual atmospheric contamination in the ACORN mode 1.5 apparent surface reflectance spectra. For each flight day, the multiplicative correction factors derived by using the AVIRIS flight line over the calibration site that day were applied to all flight lines collected on that particular day.

The resultant RTGC data from the low altitude collections appeared very well-calibrated throughout the four detectors of the AVIRIS sensor, with the exception of residual spikes at the land/water interface in some portions of the AVIRIS flight lines collected on September 14 and October 4. The RTGC data from the medium altitude collection on July 31 appeared well calibrated in the last two detectors of the AVIRIS sensor, covering wavelengths from 1.3 to 2.5 μm. However, spectral features caused by light reflected from adjacent grass fields were observed in the first two detectors of the AVIRIS/ER-2 data, covering wavelengths from 0.4 to 1.3 μm. The adjacency effect in the July 31 data was likely a result of the heavy aerosol load and patchy cloud cover in conjunction with the coarseness of the ground instantaneous field of view (GIFOV) in relation to the ground calibration site (Tanré et al., 1987). Despite ground calibration, some channels in the AVIRIS RTGC data contained artifacts that limited their use in a spectroscopic interpretation of the surface material in a pixel; thus, they were not used in spectral analyses of the RTGC data. Within regions of strong atmospheric absorption or scattering, poor sensor response, and low solar flux, these channels included 1–3, 31–33, 44, 62, 81–85, 96–97, 107–114, 153–168, 173–175, and 223–224.

Individual flight lines were geocorrected (Boardman, 1999) and further georeferenced to NAIP air photos collected in 2010. In the georeferencing procedure for each flight line, 21 to 43 ground control points were selected in the AVIRIS image and the base image. A mosaic of National Agriculture Imagery Program (NAIP) 2010 air photos was used as the base image. A 1st degree polynomial warp was used to grid the AVIRIS data to 3.5 m pixel spacing in a Universal Transverse Mercator (UTM) projection, zone 16N, WGS-84 datum. For July 31 AVIRIS/ER-2 images with a nominal input GIFOV of 7.8 m, the root-mean-square-error (RMSE) of the warping procedure averaged 9.6 m. For the September 14 and October 4 AVIRIS/Twin Otter images, with a nominal input GIFOV of 3.5 m, the RMSE of the warping procedures averaged 3.5 and 4.3 m, respectively.

2.4. MICA spectral feature comparison

MICA spectral feature comparisons are done on absorption features in spectra of materials listed in a reference spectral library. MICA uses continuum removal (Clark & Roush, 1984) and linear regression of the features in the spectrum being analyzed and reference spectral features to quantify the comparison. The wavelength regions

Table 1
Reference spectra and material descriptions with absorption feature definitions.

Name and description	Feature 1			Feature 2			Feature 3		
	Weight	Left cont. (μm)	Right cont. (μm)	Weight	Left cont. (μm)	Right cont. (μm)	Weight	Left cont. (μm)	Right cont. (μm)
Oiled-Plants3									
Oil coated leaves of *P. australis*. Spectrum has strong 1.72 and 2.30 μm absorption features arising from C – H bonds in weathered oil. Sample collected July 8, 2010, from site DWO-2-DEL-04, described in Kokaly et al. (2011). Measured in the laboratory on July 11, 2010.	0.25	1.670 to 1.685	1.765 to 1.782	0.75	2.235 to 2.250	2.380 to 2.400	n/a	n/a	n/a
Oiled-Plants2									
Oil coated leaves of *S. alterniflora* and *J. roemerianus*. Spectrum has weak chlorophyll absorption feature but strong 1.72 and 2.30 μm absorption features arising from C – H bonds in weathered oil. Sample collected from site DWO-2-BAT-09 on July 10, 2010, as described in Kokaly et al. (2011). Measured in the laboratory on July 11, 2010. A photo of the area is shown in Fig. 8.	0.25	1.670 to 1.685	1.765 to 1.782	0.75	2.235 to 2.250	2.380 to 2.400	n/a	n/a	n/a
Oiled-Plants1									
Oil coated leaves of *S. alterniflora* and *J. roemerianus*. Spectrum has very weak chlorophyll absorption feature but strong 1.72 and 2.30 μm absorption features arising from C – H bonds in weathered oil. Sample collected from site DWO-2-BAT-08 on July 10, 2010, as described in Kokaly et al. (2011). Measured in the laboratory on July 11, 2010.	0.25	1.670 to 1.685	1.765 to 1.782	0.75	2.235 to 2.250	2.380 to 2.400	n/a	n/a	n/a
Oiled-Dry-Marsh									
Oiled canopy of *S. alterniflora* and *J. roemerianus* near edge of the marsh. Portions of the canopy were non-oiled, brown leaves and stems. The spectrum has strong 1.72 and 2.30 μm absorption features arising from C – H bonds in weathered oil and a weaker 2.10 μm absorption feature from dry vegetation components. The spectrum was measured in the field on August 13, 2010, at site DWO-3-BAT-09, described in Kokaly et al. (2011).	0.25	1.652 to 1.663	1.765 to 1.782	0.75	2.220 to 2.240	2.370 to 2.385	n/a	n/a	n/a
Oiled-Marsh									
Dark, oil-coated canopy of *S. alterniflora* and *J. roemerianus* with background oil:water emulsion at edge of the marsh. Spectrum has strong 1.72 and 2.30 μm absorption features arising from C – H bonds in weathered oil. The spectrum was measured in the field on August 13, 2010, at site DWO-3-BAT-09, described in Kokaly et al. (2011).	0.25	1.652 to 1.663	1.765 to 1.782	0.75	2.220 to 2.240	2.370 to 2.385	n/a	n/a	n/a
Oil-Strong									
Black, pooled oil on the beach at Grand Isle, Louisiana. Spectrum has strong 1.72 and 2.30 μm absorption features arising from C – H bonds in weathered oil. The spectrum was measured in the field on June 9, 2010.	0.25	1.640 to 1.653	1.765 to 1.782	0.75	2.210 to 2.230	2.380 to 2.400	n/a	n/a	n/a
Veg-DrySpartina									
Brown leaves of *S. alterniflora*. Spectrum has absorption features, centered near 1.72, 2.10 and 2.27 μm, arising from leaf biochemical constituents. The spectrum was measured in the field, by using an ASD spectrometer with contact probe attachment, on June 7, 2010, at CRMS site 0322, see http://www.lacoast.gov/crms for site location and additional details.	0.25	1.652 to 1.663	1.765 to 1.782	0.75	2.210 to 2.230	2.380 to 2.400	n/a	n/a	n/a
Veg-DryPhragmites									
Brown leaves of *P. australis*. Spectrum has absorption features, centered near 1.73, 2.10 and 2.31 μm, arising from leaf biochemical constituents. The spectrum was measured in the field, by using an ASD spectrometer with contact probe attachment, on July 8, 2010, at site DWO-2-DEL-03, as described in Kokaly et al. (2011). The spectrum was saturated in the first ASD detector; channels in this wavelength range were not used in the spectral analysis.	0.25	1.652 to 1.663	1.765 to 1.782	0.75	2.210 to 2.230	2.380 to 2.400	n/a	n/a	n/a
Veg-StrongChlorophyll									
Vegetation spectrum with strong chlorophyll and leaf water absorption features. Sample and measurement described in Clark et al. (2007). Measured in the laboratory with a Beckman spectrophotometer.	0.85	0.522 to 0.552	0.737 to 0.767	0.05	0.870 to 0.900	1.063 to 1.093	0.10	1.100 to 1.131	1.265 to 1.290

for the comparisons are based on the continuum endpoints of diagnostic features in the reference spectra. Diagnostic features are strong and (or) unique features arising from chemical bonds inherent in the reference material. MICA uses an analysis framework similar to the USGS Tetracorder algorithm (Clark et al., 2003). PRISM and MICA run as a plug-in to the IDL/ENVI software (Interactive Data Language/Environment for Visualizing Images; Exelis, Boulder, Colorado).

Fig. 2 shows the diagnostic features used in this study. For oiled materials, two hydrocarbon absorption features centered near 1.72 and 2.3 μm, which arise from the C – H bonds in oil (Cloutis, 1989), were used. For the green vegetation reference spectrum, the 0.68 μm chlorophyll feature and two leaf water absorption features, centered near 0.98 and 1.2 μm, were used as diagnostic features. For dry vegetation spectra, the 2.1 and 2.3 μm absorption features arising primarily from structural biochemical constituents comprising plant

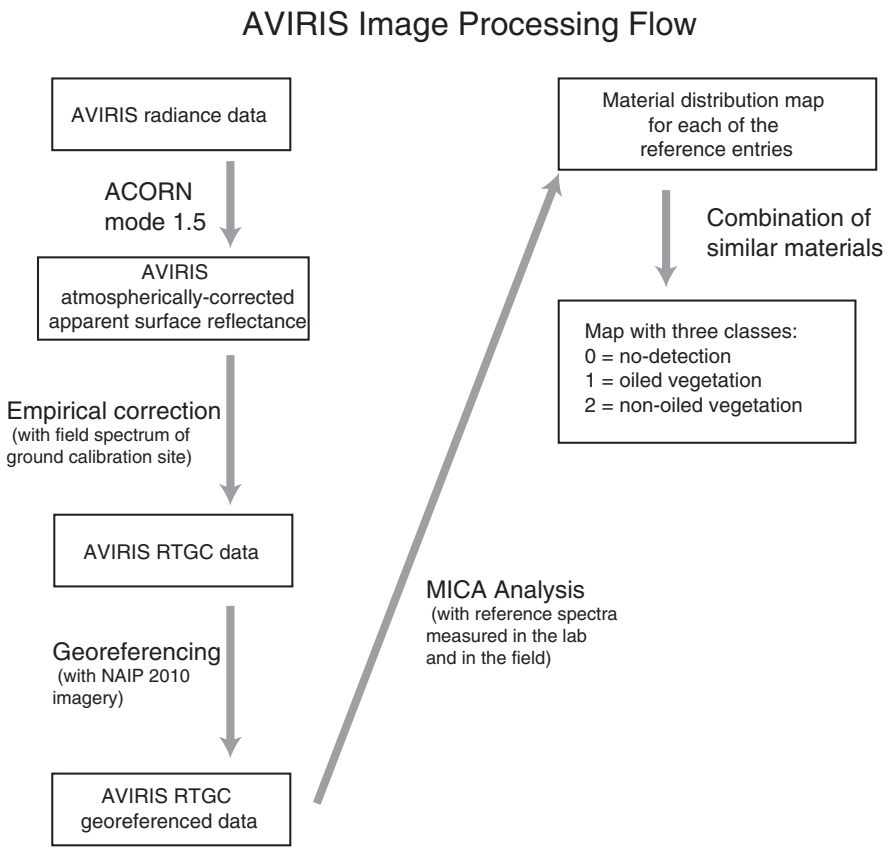

Fig. 3. Flow chart showing the steps taken in processing AVIRIS radiance data from a single date to a map of oiled marsh.

cells were used (Kokaly et al., 2009). Table 1 includes the wavelength ranges used to define the endpoints of the continua across those features. The AVIRIS channels within the wavelength ranges were averaged to establish the left and right endpoints to use in computing the equation of the continuum lines.

MICA uses the coefficient of determination (r^2) from the linear regression between the continuum-removed features in the reference spectrum and the corresponding continuum-removed regions in the spectrum being analyzed. The r^2 value is termed the feature "fit" value, where the fit is the measure of the agreement between the spectral features. Fit values range from 0 to 1, with better matches indicated by high fit numbers. A perfect agreement between the spectral features is indicated by a value of 1.

Fig. 4 shows an example of the comparison of an AVIRIS pixel spectrum to the reference spectrum of Oiled-Dry-Marsh for two spectral features, the 1.72 and 2.3 μm C–H features. In addition to a fit value, a depth value, which also ranges from 0 to 1, for the feature in the spectrum being analyzed is computed by using the reference feature scaled to the AVIRIS feature. The scaled reference feature depth is used instead of computing the depth from the AVIRIS spectrum in order to reduce the potential impact of noise in the remotely sensed spectra (Clark et al., 2003; Kokaly, 2011).

In MICA, the feature fits from multiple spectral features can be combined in a weighted average, where weighting factors can range from 0 to 1 and the sum of weights is constrained to equal 1. The weighted average is referred to as the overall fit. In the MICA spectral comparisons, the term "best match" is applied to the reference spectrum with the highest overall fit with the spectrum being analyzed. Overall values for weighted depths are also computed during the MICA analysis. An additional parameter, describing the feature comparison for each material is derived, that is, the overall fit∗depth, or F∗D. The overall F∗D is computed as the sum of the products of the weight multiplied by the fit value multiplied by the depth value for each feature.

MICA employs the concepts of optional feature and continuum constraints for each material in the command file in order to reduce false-positive identifications. Defined individually for each feature in the reference spectra, the feature constraints are threshold levels on values of fit, depth, and F∗D that must be met by the spectrum being analyzed in order to consider it as a match to the reference material. Similarly, continuum constraints for each feature, which include the reflectance levels of the left and right endpoints (R_{c1} and R_{c2}) and midpoint (R_{cmid}) of the continuum line must also be met by the spectrum being analyzed in order to consider it as a match to the reference material. Additionally, constraints on the allowable range of the ratio of the reflectance level of the right continuum endpoint to the left, R_{c2}/R_{c1}, can also be set. The feature and continuum parameters are depicted on the example AVIRIS spectrum in Fig. 4. Material constraints on overall fit, depth and F∗D can also be set for each reference entry in the MICA command file (see Kokaly, 2011).

For the detection of oiled marsh, the MICA command file, which lists the reference spectra, continuum and feature constraints, is included in the supplementary data. The reference materials and continuum endpoints used to define the spectral features are given in Table 1, along with feature weighting factors. For oiled materials and dry vegetation, a higher weighting factor (0.75) was given to the 2.3 μm feature compared to the 1.72 μm feature (with a weighting factor of 0.25). Higher weight was given to the 2.3 μm feature for several reasons: 1) the feature appeared visually more distinct between the spectra of oiled marsh compared to the non-oiled vegetation, and 2) residual atmospheric contamination in the AVIRIS spectra appeared to more strongly impact the long-wave side of the 1.72 μm feature compared to the 2.3 μm feature.

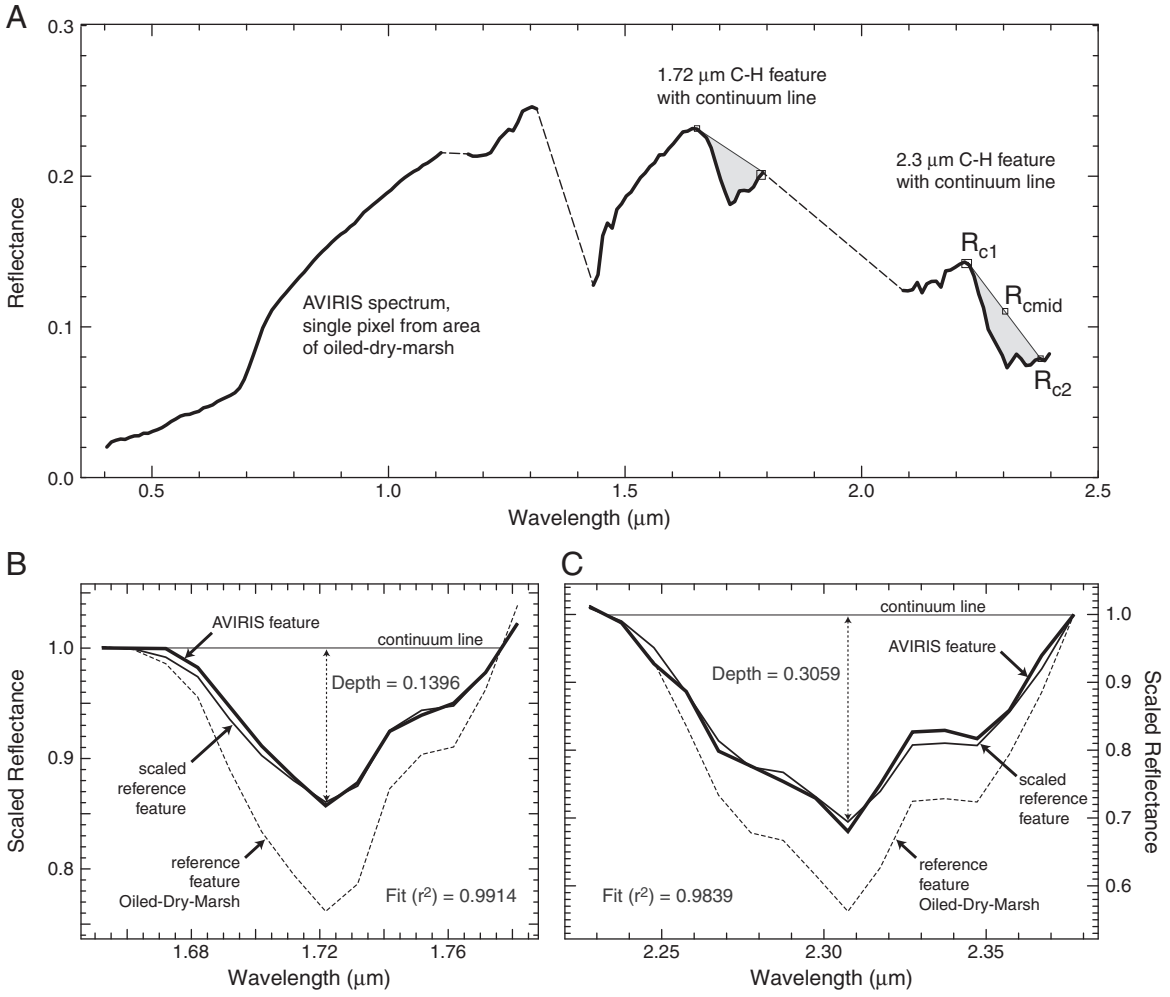

Fig. 4. A) Extracted spectrum from AVIRIS data for a pixel equivalent to the collection location of the Oiled-Dry-Marsh spectrum. The continuum lines of the 1.72 μm and 2.3 μm C – H absorption features are marked on the spectrum. The left, midpoint, and right continuum reflectance levels of the 2.3 μm feature are indicated on the spectrum. B) The continuum-removed 1.72 μm feature of the AVIRIS pixel compared to the Oiled-Dry-Marsh reference feature, including the MICA fit and depth values for this feature. C) The continuum-removed 2.3 μm feature of the AVIRIS pixel compared to the Oiled-Dry-Marsh reference feature, including the MICA fit and depth values for this feature.

The constraints used for each feature are given in Table 2. The reflectance levels of the midpoints in the continuum lines were required to be greater than 0.02, in order to avoid false positives that might be caused by noise in dark pixels. A maximum value of 1.25 was used as a threshold for the ratio of the reflectance values of the right continuum to the left continuum for the 1.72 μm features. A maximum value of 1.0 was used

Table 2
Continuum and feature constraints used in the MICA command file.

Material name	Feature name	Left refl. level	Mid refl. level	Right refl. level	Ratio left. divided by right	Fit	Depth
Veg-StrongChlorophyll	0.68 μm chlorophyll feature	n.s.	>0.05	n.s	>0.9	>0.80	>0.675
	0.98 μm leaf water feature	n.s.	>0.10	n.s	n.s.	n.s.	n.s.
	1.20 μm leaf water feature	n.s.	>0.10	n.s	n.s.	n.s.	n.s.
Oiled-Plants3	1.72 μm C – H feature	n.s.	>0.02	n.s	<1.25	>0.55	>0.0075
	2.30 μm C – H feature	n.s.	>0.02	n.s	<1	>0.55	>0.0075
Oiled-Plants2	1.72 μm C – H feature	n.s.	>0.02	n.s	<1.25	>0.55	>0.0075
	2.30 μm C – H feature	n.s.	>0.02	n.s	<1	>0.55	>0.0075
Oiled-Plants1	1.72 μm C – H feature	n.s.	>0.02	n.s	<1.25	>0.55	>0.0075
	2.30 μm C – H feature	n.s.	>0.02	n.s	<1	>0.55	>0.0075
Oiled-Marsh	1.72 μm C – H feature	n.s.	>0.02	n.s	<1.25	>0.55	>0.0075
	2.30 μm C – H feature	n.s.	>0.02	n.s	<1	>0.55	>0.0075
Oiled-Dry-Marsh	1.72 μm C – H feature	n.s.	>0.02	n.s	<1.25	>0.55	>0.0075
	2.30 μm C – H feature	n.s.	>0.02	n.s	<1	>0.55	>0.0075
Veg-DryPhragmites	1.72 μm C – H feature	n.s.	>0.02	n.s	<1.25	>0.55	>0.0075
	2.30 μm C – H feature	n.s.	>0.02	n.s	<1	>0.55	>0.0075
Veg-DrySpartina	1.72 μm C – H feature	n.s.	>0.02	n.s	<1.25	>0.55	>0.0075
	2.30 μm C – H feature	n.s.	>0.02	n.s	<1	>0.55	>0.0075
Oil-Strong	1.72 μm C – H feature	n.s.	>0.02	n.s	<1	>0.55	>0.0075
	2.30 μm C – H feature	n.s.	>0.02	n.s	<1	>0.55	>0.0075

n.s. indicates constraint was not set.

as a threshold for this ratio for the 2.3 μm features. These thresholds on the ratio of the continuum endpoints were established so that only the spectra that have continuum lines with a negative slope across the 2.3 μm feature are considered as best matches. Similarly, the analyzed spectra cannot have more than a slightly positive slope across the 1.72 μm feature in order to be matched to the materials. These thresholds were determined by an examination of the trends in values in the continuum lines for the reference spectra and for other field spectra used for validation of the MICA algorithm (see Section 2.4).

An overall threshold fit value of 0.6 was required for the fits to the reference spectra of all materials except for Veg-StrongChlorophyll, which had a threshold of 0.8. Overall feature depths were required to be greater than a threshold value of 0.0125 for all materials except for Veg-StrongChlorophyll, which had a depth threshold of 0.6.

Additional entries for the dry vegetation reference spectra were made that used only the 2.3 μm feature (weighted by 1.0) as a reference feature. To identify the matches to these entries in the MICA command file, they were designated with the following output names, "Veg-DrySpartina_2_3micron" and "Veg-DryPhragmites_2_3micron". Thus, there were 11 total reference entries in the MICA command file. The repeated entries for the dry vegetation reference spectra were made because the shapes and band center positions of the shortwave-infrared (SWIR) absorption features in leaves change as water content increases (see Kokaly & Clark, 1999; Kokaly et al., 2009). Using the same radiative transfer modeling approach as those studies, a rice leaf spectrum was modeled with water contents of 5, 10, 20, 30, 40, 50, 50, 60, 70, and 80% (see Fig. 5A). The vegetation absorption features centered near 1.72, 2.1 and 2.3 μm were continuum-removed (see Fig. 5B–D).

The 1.72 μm feature becomes quite distorted as leaf water content increases, changing from an absorption feature centered at 1.725 μm arising from the leaf biochemical constituents to a feature centered at 1.774 μm. This change becomes noticeable at modeled water contents greater than 20% (see Fig. 5B). As a way of quantifying the degree of change, the spectral feature of the dry leaf spectrum was compared to each of the modeled leaf spectra with added water by using MICA's linear regression, the resulting fit values are depicted in Fig. 5. The fit value decreases from 0.987 for 5% water content to 0.847 for 20% water content; modeled leaf spectra with 30% and greater water content have very altered shapes compared to the dry leaf spectrum as evidenced by the rapid decrease in fit values.

As water content increases, the 2.1 μm feature, shown in Fig. 5C, does not become as distorted as the 1.72 μm feature. At 30% water content, the fit value to the dry leaf spectrum is 0.956. However, the fit drops to 0.739 at 40% modeled leaf water. At 50% water content, the feature turns from an absorption feature to an emission feature (emission being the term applied to features that have reflectance values above the continuum line).

In contrast to the dry leaf features centered at shorter wavelengths in the SWIR region, the shape of the 2.3 μm feature remains relatively unaltered despite an increase in water content (see Fig. 5D). At 40% modeled leaf water content, the fit value to the dry leaf feature remains high at 0.983. The fit value drops slightly more, to 0.923, at 50% modeled water content. At 70% and 80% water content, the

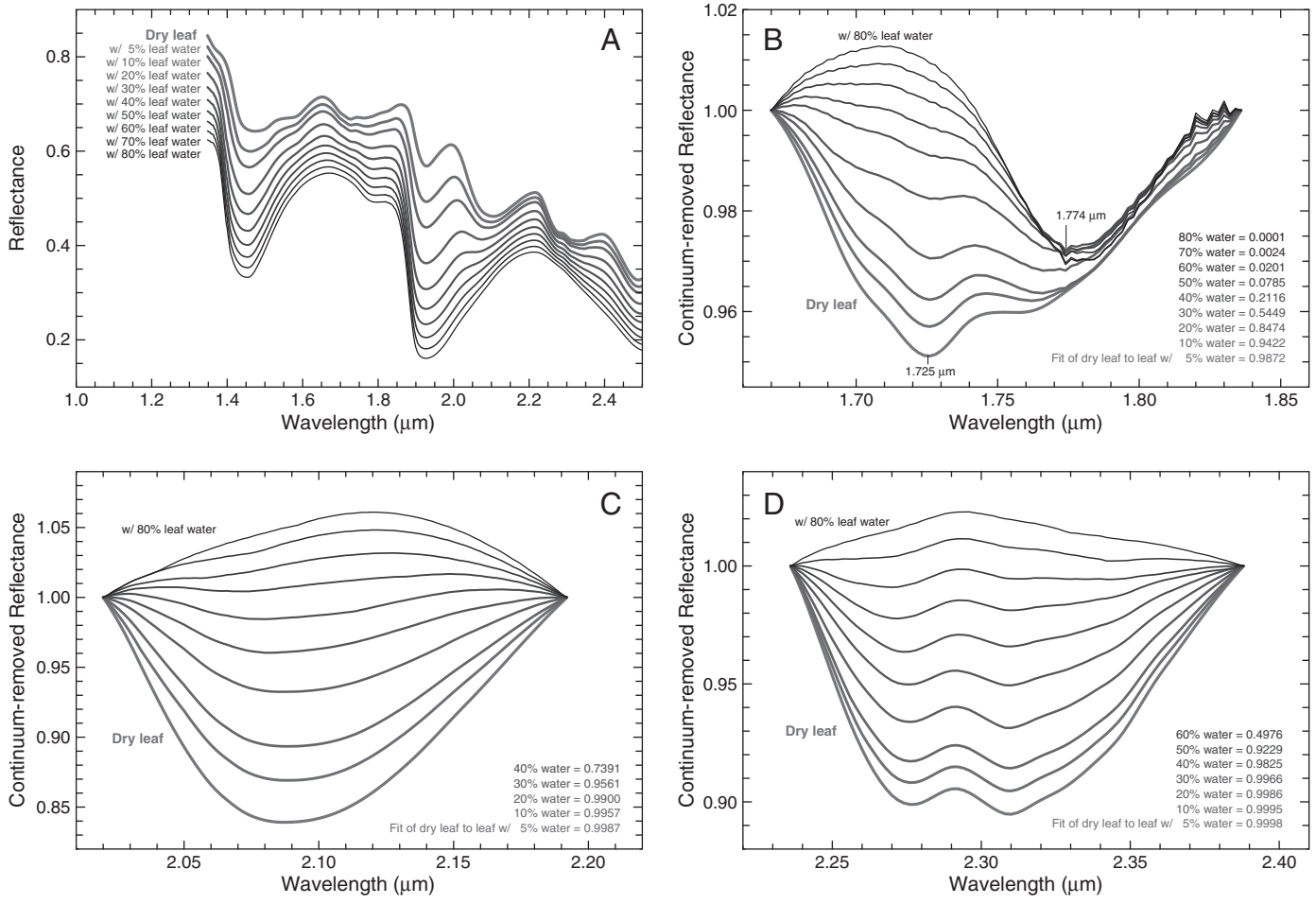

Fig. 5. A) Dry leaf spectrum and modeled leaf spectra with an increase in water content. B) Continuum-removed 1.72 μm feature. C) Continuum-removed 2.1 μm feature. D) Continuum-removed 2.3 μm feature. MICA fit values of the dry leaf feature compared to features in modeled leaf spectra are shown for absorption features.

reflectance values fall above the continuum line and the feature changes from being characterized as an absorption feature to an emission feature. Thus, it is clear that as water content increases, the 2.3 μm absorption features, arising from biochemical constituents such as protein, cellulose and lignin, are better preserved in the leaf spectra compared to the 1.72 and 2.1 μm features. For this reason, additional entries for the two dry vegetation reference spectra were made by using only the 2.3 μm feature.

For each date of the AVIRIS data, the output MICA material images, showing the distribution of pixels which were the best match to each entry in the reference spectral library, were combined into a summary classification image. The summary classification images were made by assigning pixels that matched any of the reference spectra of the oiled materials to a single class value and color; similarly, a specific class value and color were assigned to all pixels that matched any of the reference spectra of the non-oiled vegetation.

2.5. Map development and compositing

The coverage in flight lines from individual dates suffered from either cloud contamination or gaps in coverage over Barataria Bay; thus, a composite oil map was produced from the three images to make a comprehensive map of oiling in the area. The first steps in the procedure were to mask the cloudy portions of the images and rectify their pixels by using the ENVI "layer stack" function. The next step in the procedure was to assign pixels in the composite map the class value for vegetation for any pixel where any of the three images had the vegetation class value. Subsequently, pixels in the composite map were assigned the oiled marsh value if any of the three images had the oiled marsh class. As a result, the simple composite map preferentially portrays all pixels of oiled marsh detected in any of the three image dates. Fig. S1 in the Supplementary data shows the steps of the compositing procedure.

The simple composite map was further processed to differentiate the oil detections in each pixel into four separate classes based on the spatial contiguity of oil with adjacent pixels and temporal persistence in multi-date images. The further processing differentiates oiled marsh pixels detected sporadically, in both spatial and temporal domains, from areas of widespread continuous oil coverage and temporally persistent oiling. In the first step of this processing, a spatial filter was run to produce an intermediate "sieved" composite map; pixels mapped as oiled marsh that did not have at least two of the neighboring eight pixels identified as oiled marsh, were reclassified as non-oiled in the sieved map. To create the composite oil probability map, the simple composite map, the sieved composite map, and the three rectified oil maps from the collection dates were synthesized according to the criteria shown in Fig. S1. The oiled marsh probability class image preserves the entirety of pixels in which oil was detected but adds additional information on the likelihood of those pixels being oiled either due to spatial contiguity and/or repeated detection.

Because it is difficult to see the details in the 3.5 m pixels over the large study area, the raster-based oiled marsh class image was converted to vector data. To further simplify the portrayal of information at a broad scale, all three higher probability classes were combined into a single class. This form of the map was used for spatial analysis to compute statistics on the linear extent of oiled marsh on the coastline and the average lateral distance of penetration of oil into the marsh from the shoreline. The linear extent of the coastline covered by each polygon of high probability oiled marsh was measured and the extent of each oiled patch was summed to calculate the total extent of oiled coastline in this class. The number of low probability shoreline pixels was totaled and multiplied by the composite map grid spacing, 3.5 m, to calculate the extent of oiled coastline in this class. The lateral distance of penetration of oil was calculated from the closest shoreline or observable water pathway greater than 49 m in width. Transect lines at regular 5 m intervals were created running perpendicular to the shoreline and the distance to the back of the oiling was calculated using a Euclidean distance algorithm.

2.6. Field spectra for algorithm validation

In addition to the reference oiled materials and non-oiled vegetation spectra in the reference spectral library, ASD FS3 field spectra at 65 other sites containing a diversity of materials (see Tables S1 and S2 in the Supplementary data) were collected during the field surveys made from May to August, 2010. Reflectance measurements of 37 targeted materials of a single type were made, including oiled marsh plants, oil emulsions on marsh sediments, green and non-photosynthetic vegetation, beach sand, marsh sediment (mud), and water (see Table S1). Reflectance measurements of 28 areas of mixed vegetation species at CRMS monitoring plots were also made. Species in these plots included *S. alterniflora*, *Spartina patens*, *D. spicata*, *Schoenoplectus americanus, Schoenoplectus robustus*, *Lythrum lineare*, *Polygonum punctatum*, and other species that occurred infrequently with small values of cover (see Table S2). Cover by vegetation species and the dominant background materials were determined at 2×2 m subplots of CRMS sites 0121, 0322, and 0326. Using sunlight as the source of illumination, twenty field spectra at each vegetation subplot were recorded. When cloud cover interfered with proper measurement using reflected sunlight, the spectra were measured using the ASD FS3 with the contact probe. In the vegetation subplots, plant stems and leaves in the top 30 cm of the canopy were bunched together and the contact probe pressed against the optically thick bundle. For each bunch, a spectrum was recorded at two different positions along the bunch. Typically, ten bundles (20 spectra) in each subplot were recorded for subsequent averaging.

Selected examples from the validation spectra are shown in Fig. 6. In Fig. 6A, strong 1.72 μm and 2.3 μm features are evident in both the spectra of the oiled materials and dry vegetation. Fig. 6B, illustrates the variability in chlorophyll and leaf water absorption features and reflectance levels. The variability arises, in part, from variations in canopy cover, species composition, and background materials (for example, water, wet marsh sediment, and dry marsh sediment).

In light of the variability in vegetation spectra, MICA analysis was applied to the 65 validation spectra to test its ability to reliably discriminate between oiled and non-oiled materials. Each validation spectrum was categorized as oiled or non-oiled. The best match to each spectrum, resulting from the MICA analysis, was also classified as oiled or non-oiled. A correspondence in the actual class of a validation spectrum and the class of the matching spectrum was considered a successful result. An error in the MICA analysis was defined as a MICA result where the best match differed in class (oiled vs. non-oiled) from the actual material class (e.g., if the spectrum of a non-oiled area of vegetation matched an oiled plant spectrum). Non-oiled, non-vegetation materials, such as wet sand, that were not classified, that is, all matches to the reference spectra fell below the material fit thresholds, were considered a successful result.

2.7. Map accuracy assessment

Accuracy assessments of the AVIRIS results were made by using data from field surveys conducted on July 7–10, August 12–14, and August 24–26, 2010 (Kokaly et al., 2011). Survey points where oil coated vegetation and oil-damaged canopy were observed were considered as reference oiled locations. Survey points where oil was observed on only basal portions of the stems of intact canopies or where no oil was observed were used as reference non-oiled locations; see Kokaly et al. (2011) for detailed information on survey points. Considering the geocorrection uncertainties of the AVIRIS data and the accuracy limits of the GPS locations of the survey points

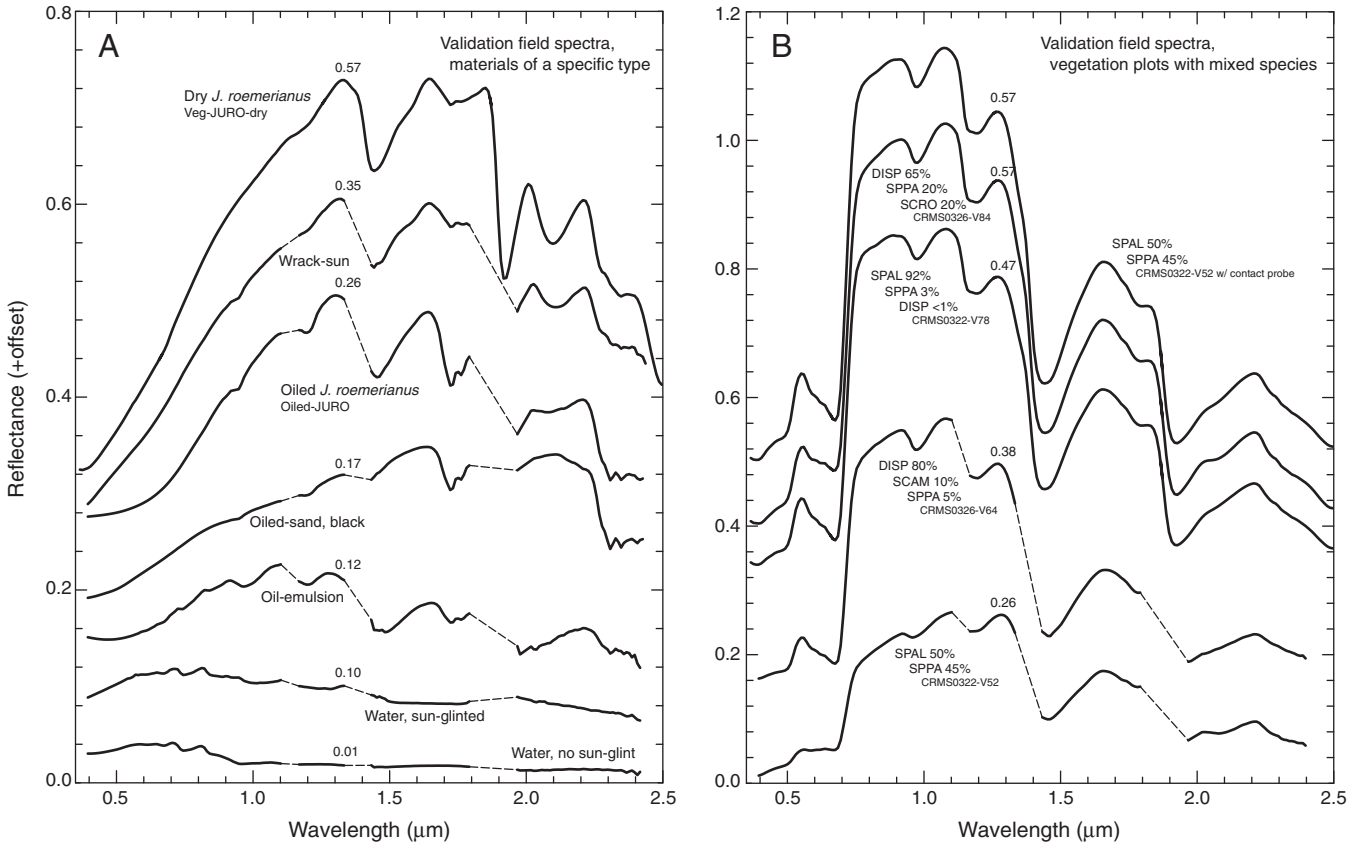

Fig. 6. Example field spectra used for validating the MICA method to discriminate oiled and non-oiled vegetation: A) spectra of targeted materials of a specific type. The spectra are offset for clarity; the additive offset factors are 0, 0, 0.1, 0.15, 0.25, 0.25, and 0.35 for the spectra from bottom to top. B) Spectra of vegetation of mixed species. The spectra are offset for clarity; the additive offset factors are 0, 0.25, 0.3, 0.35, and 0.4 for the spectra from bottom to top. Channels in wavelength regions of strong atmospheric absorption were deleted from field spectra measured with sunlight as the illumination. These regions in the spectra are shown with a thin, dashed line.

(typically 5 m), multiple pixels were evaluated for the presence/absence of oil in relation to field observations at survey points. For a survey point at the shore, the pixel containing the survey point and its surrounding pixels were evaluated. If oil was found in one or more of these nine pixels, the remote sensing result for oil at that survey point was considered to be oiled. If oil was not detected in any of these pixels, the remote sensing result for oil at that survey point was non-oiled. If the survey point was offshore, the three closest shoreline pixels in the image were evaluated in a similar manner. Standard error matrices (Congalton & Mead, 1983) were constructed to assess the accuracy of oil and non-oiled classes in the oil maps.

2.8. Spatial and spectral resampling and mixture analysis

Spatial and spectral resampling of the October 4, 2010, AVIRIS data at 3.5 m GIFOV was performed to examine the impact of spatial and spectral resolutions on the ability to detect oiled marsh. Spatial resampling to produce AVIRIS data at 30 m GIFOV was performed by aggregating the high resolution pixels. MICA analysis was applied to the 30 m AVIRIS data.

Spectral resampling of 3.5 and 30 m AVIRIS data to Landsat 7 ETM data was done by using the spectral resampling function in ENVI (see Fig. S2 in the Supplementary data to view the resampled reference spectra). Because the diagnostic C–H features at 1.72 and 2.3 μm are not resolved in Landsat spectra, a different approach, multiple endmember spectral mixture analysis (MESMA: Roberts et al., 1998; Dennison & Roberts, 2003), was used to classify the imagery. By using the simulated Landsat data, image-based spectral libraries for MESMA were built by extracting a window of pixels around the dominant vegetation types as delineated in Sasser et al. (2008). Library entries for water and sun-glinted water were extracted from the AVIRIS data. Selection of endmembers for oiled marsh was guided by a spectral examination of the 2.3 μm C–H absorption feature in AVIRIS data. Pixels that had a deep 2.3 μm absorption feature were added to the spectral library as endmembers for the MESMA analysis. An iterative selection of the spectra was performed to identify the spectra that best modeled the spectra within the class and minimized confusion between classes (Keely Roth, personal communication). These "best spectra" were applied to the imagery, with the endmember having the lowest RMSE being selected for any given pixel. As with the MICA analysis, the individual class results from MESMA were combined into simplified classes of materials (oiled marsh, non-oiled vegetation, water, and sunglint). Note: the image-based spectral library for MESMA applied to the simulated Landsat data is distinct from the spectral library used for MICA analysis of the AVIRIS data.

3. Results

3.1. Field observations in oiled marshes

Field observations at the 61 survey points in the Barataria Bay marshes (Fig. 7) showed a range in oil impacts on the dominant species, *S. alterniflora* and *J. roemerianus* (Kokaly et al., 2011). In addition to oil on the plants, oil was observed on the marsh sediment at some sites in Barataria Bay, both above and below the water surface depending on the level of the tide. Oil adhered to marsh sediments and oil coatings on vegetation persisted in the marsh from the earliest

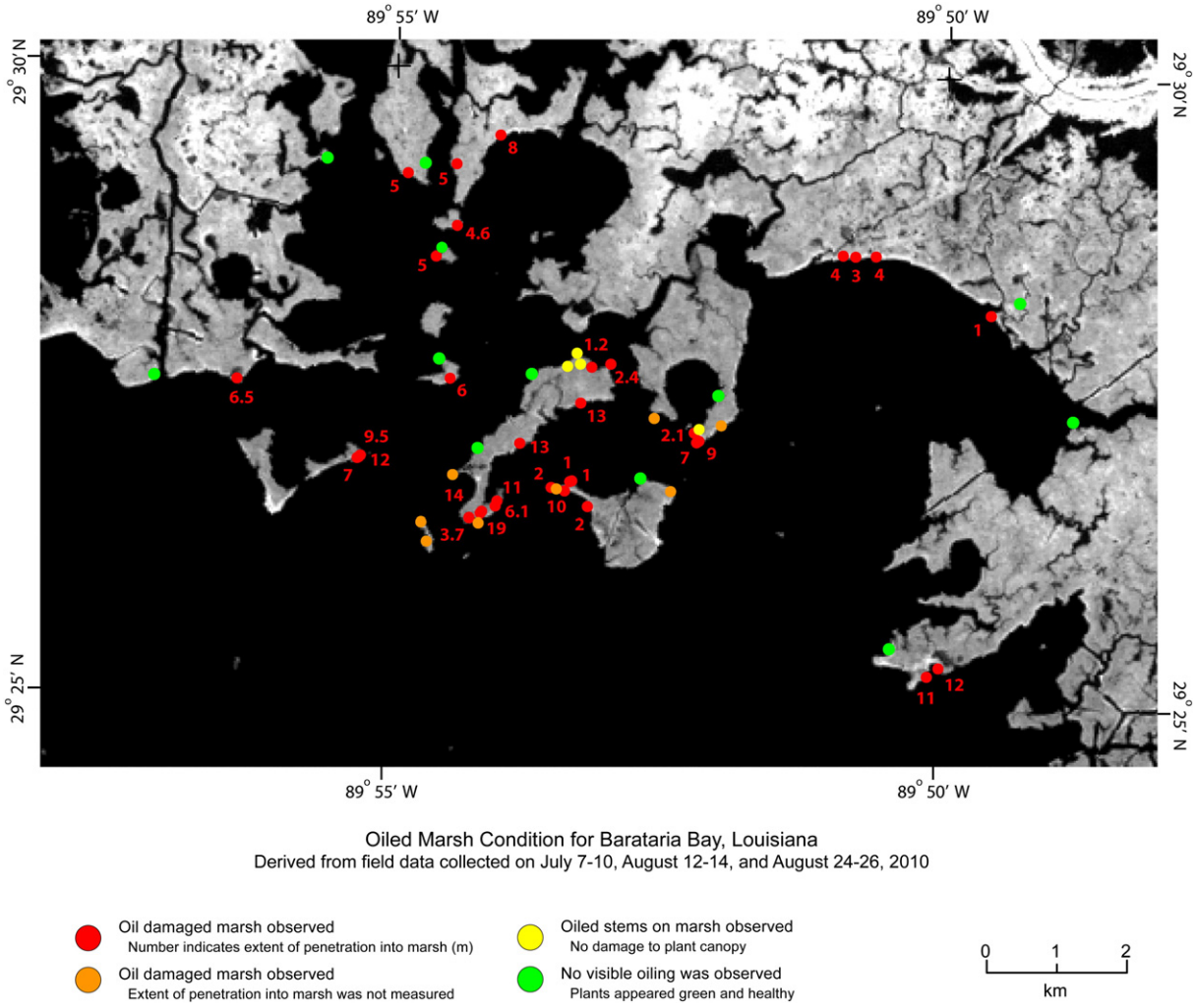

Fig. 7. Survey points in the Bay Jimmy subarea with oil damage indicated by color codes: green indicates that oil was not observed, yellow indicates that oil was found on stems of plants, orange indicates that oil-damaged canopy was observed but the depth of penetration of the oil-damaged zone was not measured, and red indicates that oil-damaged canopy was observed and the adjacent number indicates the extent (in meters) that the oil damage extended into the marsh.
Adapted from Kokaly et al. (2011).

field survey (July 7) to the latest airborne survey (October 4). The persistence of oil contamination and the observation of oil sheen in the water at most oiled sites suggest that some oil constituents may be available for further transport into the marsh by tides and wind, which may cause future impacts. Vegetation with oiled stems and water contaminated with oil sheen and red-brown oil water emulsions were observed in narrow interior waterways.

Progressive vegetation degradation was observed at sites repeatedly visited in Barataria Bay. Oiled plant stems and leaves laid over by the weight of the oil eventually broke and were removed through tidal action. In these areas, cover was reduced to a zone of 2–5 cm high dead plant stems at the edge of the marsh. As described in Kokaly et al. (2011) visual signs of degradation and recovery varied by site. Fig. 8 shows photos from field survey sites of oil-damaged canopy, oiled sediment, marsh edge exposed to erosion, and vegetative regrowth.

The DOC concentrations (Table 3) for visibly oiled sites ($n=8$) ranged from 6.1 to 19.5 mg/L DOC. The DOC concentrations from open water sites 10 s of meters offshore ($n=2$) ranged from 7.6 to 7.8 mg/L DOC. The DOC concentrations at visibly unoiled sites ($n=2$; 8.4–9.1 mg/L DOC) were similar to the concentrations at visibly oiled sites with the exception of one visibly oiled site, DWO-4-BAT09. This site had a much greater DOC concentration (19.5 mg/L DOC) compared to the others ($\leq$8.41 mg/L DOC).

3.2. Evaluation of AVIRIS reflectance retrieval and comparison to reference spectra

Success in converting AVIRIS radiance to RTGC reflectance was evaluated by using spectra extracted from the AVIRIS data at locations equivalent to the places at which the reference spectra were measured or where the reference samples were collected (Oiled-Plants2, Oiled-Plants-1, Oiled-Marsh, Oiled–Dry-Marsh, and Veg-DrySpartina). Notes from the field surveys were used to guide the selection of sites analogous to the Veg-StrongChlorophyll and Oil-Strong reference materials. Since the *P. australis* spectra (Oiled-Plants3 and Veg-DryPhragmites) were not from the Barataria Bay area, the RTGC spectra could not be extracted. A single pixel spectrum was extracted from each area analogous to the location of the reference spectra (see Fig. 9). In comparison to the reference spectra, the extracted pixel spectra have the same overall shapes and spectral features (compare Figs. 2 and 9).

For quantitative comparison of the similarity in the spectral features, MICA analysis was conducted on each extracted AVIRIS spectrum. The overall fit results are shown in Table 4. With the exception of the

Fig. 8. Photos of oiled marsh sites in northern Barataria Bay, as described in Kokaly et al. (2011). The upper left photo, taken on July 10, 2010, at site DWO-2-BAT-09, shows dark reddish-brown areas of oiled plants and damaged canopy that penetrated up to 4.6 m into the marsh, species were primarily *S. alterniflora* and *J. roemerianus*. The bottom left photo, taken on July 10, 2010, at site DWO-2-BAT-11, shows dark red blotches below the water level. These are areas of submersed oil which had adhered to the marsh bottom. The bottom right photo, taken on August 13, 2010, at site DWO-3-BAT-08, shows a 15 cm zone of dead, broken plant stems found at the eroded marsh edge. The upper right photo, taken on August 26, 2010, at site OBS-4-BAT-04, shows green shoots of *S. patens* and *D. spicata* regeneration within the oiled zone.

Oiled-Marsh spectrum, the best fit to each extracted remotely-sensed spectrum was the corresponding reference field/lab spectrum. For the Oiled-Marsh spectrum, the fit to its corresponding reference spectrum was 0.976; however, the fit of that extracted spectrum to Oiled-Dry-Marsh was higher, at 0.986. Table 4 shows that, in general, the analyzed AVIRIS pixel spectra in oiled areas have higher fit values to the reference spectra of oiled materials compared to non-oiled materials. The AVIRIS pixel spectra in the non-oiled areas have higher fit values to the reference spectra in the non-oiled category.

A comparison of the absorption features in the AVIRIS pixel spectrum from the Oiled-Dry-Marsh location to the reference spectra of the oiled materials and the non-oiled vegetation is shown in Fig. 10. The feature comparisons show that the AVIRIS Oiled-Dry-Marsh pixel spectrum is more similar to the reference spectra of the oiled materials in the 2.3 μm feature (with fits of 0.984 and 0.950) than to the reference spectra of the non-oiled vegetation (with fits of 0.881 and 0.876). The comparisons of the 1.72 μm feature show the highest fit to be to the Oiled-Dry-Marsh spectrum (0.991); however, the next highest fit is to Veg-DrySpartina (0.941). As discussed in Section 2.4, the greater distinction in the 2.3 μm region between the spectra of the oiled marsh compared to the non-oiled vegetation is part of the basis for a higher weighting on the 2.3 μm feature (weighted by 0.75) compared to the 1.72 μm feature (weighted by 0.25).

Table 3
Dissolved organic carbon (DOC) concentrations in Barataria Bay water samples collected August 24–26, 2010.

Site	Latitude (deg. N)	Longitude (deg. W)	Site condition	DOC (mg/L)
DWO-4-BAT01	29.44831	89.92112	Oiled marsh	8.2
DWO-4-BAT05	29.46070	89.88640	Open water	7.8
DWO-4-BAT06	29.45116	89.86999	Oiled marsh	7.0
DWO-4-BAT09	29.48598	89.91483	Oiled marsh	19.5
DWO-4-BAT10	29.48723	89.91228	Marsh, no visible oiling	9.1
DWO-4-BAT12	29.45748	89.86707	Marsh, no visible oiling	8.4
DWO-4-BAT13	29.48723	89.90720	Oiled marsh	8.4
DWO-4-BAT13F	29.48720	89.90720	Open water	7.6
DWO-4-OBS02	29.42191	89.83297	Oiled marsh	8.1
DWO-4-OBS04	29.49129	89.90100	Oiled marsh	7.8
DWO-4-OBS07	29.47507	89.91019	Oiled marsh	6.1
DWO-4-OBS11	29.44450	89.87408	Oiled marsh	6.7

3.3. Validation of MICA analysis with field spectra

All seven validation spectra of the oiled materials had their best match to the reference spectra of the oiled materials (see Table 5); fit values ranged from 0.917 to 0.992. There was no confusion with the reference spectra of non-oiled vegetation. All 18 of the validation spectra of non-oiled plants of single species were matched to reference spectra of the non-oiled vegetation (with fit values to the best matched material ranging from 0.822 to 0.996). The validation spectra of the non-oiled plants of mixed species were all matched to reference spectra of non-oiled vegetation. The fit values of these 28 spectra to their matched reference spectra ranged from 0.661 to 0.997. None of the non-oiled, non-vegetation validation spectra were matched to any of the reference spectra.

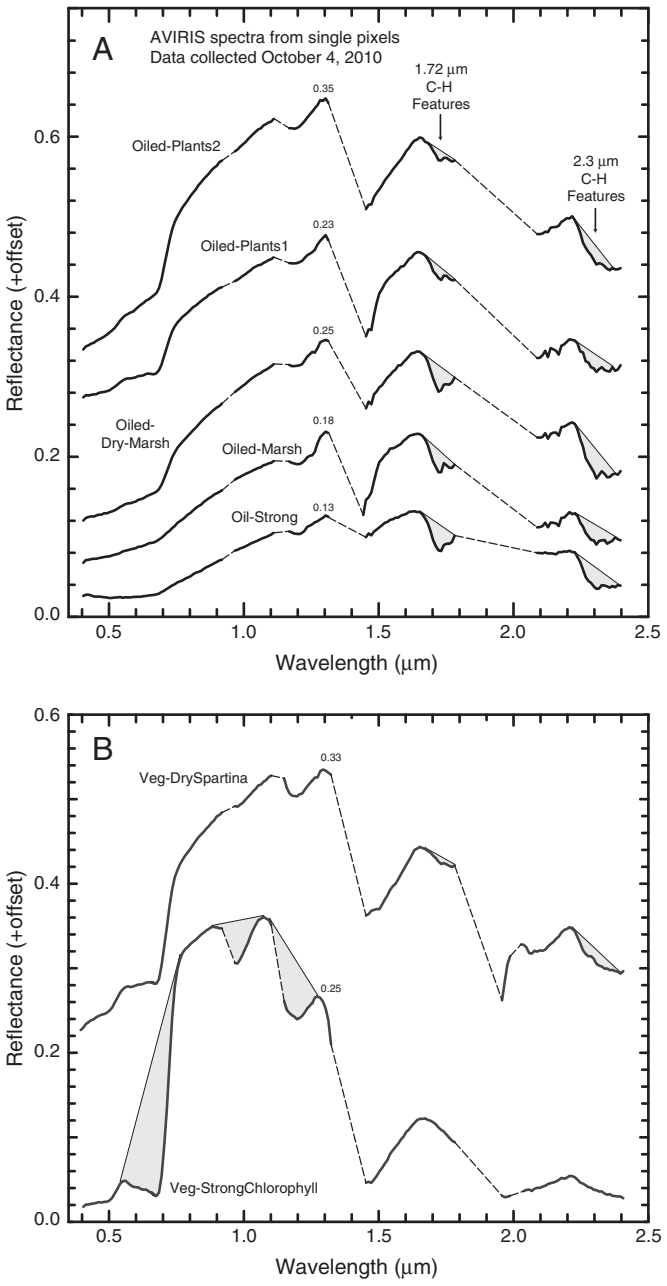

Fig. 9. Extracted AVIRIS spectra from single pixels at locations equivalent to the reference spectra (see Fig. 2). A) Spectra of oil, oiled plants and marsh. The spectra are offset for clarity; the additive offset factors are 0, 0.05, 0.10, 0.25, and 0.30 for the spectra from bottom to top. B) Reference spectra of non-oiled vegetation. The spectra are offset for clarity; the additive offset factors are 0 and 0.20 for the spectra from bottom to top. Continuum lines across the diagnostic absorption features defined in the MICA command file are shown with a thin line. The corresponding areas of the absorption features are shaded in light gray. Channels in wavelength regions of strong atmospheric absorption were deleted from field spectra measured with sunlight as the illumination. These regions in the spectra are shown with a thin, dashed line.

3.4. Maps of oiled marsh — Barataria Bay

Visual examination of the vector form of the composite map for the Barataria Bay study area (Fig. 11) shows that the majority of the oiled marsh was distributed in narrow shoreline zones. The vector map allows the oiling to be depicted across the study area in a discernible way; however, it overemphasizes the oiled areas of a single pixel or several pixels. A subset of the original raster-based maps of the analyzed AVIRIS data is shown in Fig. 12 for the Bay Jimmy subarea. Fine details are better portrayed in the raster map at this scale. Foremost among the regions with concentrations of the oiled marsh, is the Bay Jimmy subarea in northern Barataria Bay. Of all the pixels detected as oiled marsh by the MICA analysis, 79.3% of them were in this area, with most of the oil in the area around Bay Jimmy, Wilkinson Bay, and Bay Batiste (see Fig. 11). Other areas of extensive oiling include Queen Bess Island and Bay Ronquille with 1.3% and 6.4% of all oiled pixels, respectively.

3.5. Accuracy assessment

Evaluating the probability classes in the composite oil probability map as a single class, resulted in 93.4% overall accuracy (Table 6). The one "false-positive" detection by the algorithm occurred for a reference point where oil was observed only on basal portions of the plant stems. An examination of the field measurements of the lateral distance of penetration at the oiled survey points showed that detection accuracy was 100% for the 39 reference points where the zone containing oil coated plants with a damaged canopy intruded more than 1.2 m into the marsh. Only one of the four oiled reference points with lower penetration was detected. Maps of oiled marsh derived from single AVIRIS image dates also had high accuracies, 89.3%, 89.8%, and 90.6%, for July 31, September 14, and October 4, 2010, respectively. As for the composite, the accuracies in detecting zones of oiling with greater than 1.2 m of penetration were high, 94.1%, 93.8%, and 94.4%, for the July 31, September 14, and October 4 AVIRIS data, respectively.

3.6. Distribution of oil

In total, 36.62 ha in Barataria Bay were classified as oiled, of which 78.4% (28.69 ha) were in the spatially contiguous and (or) temporally persistent classes (red and orange pixels in Fig. 12). Of the total oiled area, most fell in the north Barataria Bay, 27.04 ha. Other areas with substantial stretches of oiled marsh included Queen Bess Island, with 0.49 ha of oiling, and the islands in southern Barataria Bay, around Cat Bay, Bay Ronquille, and Bay Long, with 2.33 ha of oiling. Nearly all of the oiling is attributed to the Deepwater Horizon incident, with the possible exception of 2.40 ha on the northern shore of Mud Lake, near the site of the July 27, 2010, Mud Lake oil release. Oiled pixels in the vicinity of Mud Lake show a different pattern of oil inundation, a non-contiguous dotted pattern, compared to the oiled areas in the rest of Barataria Bay, which stretch in near-contiguous segments along the shoreline.

Of the total area in Barataria Bay in which oil was detected, 75.6% (27.70 ha) occurred within 20 m of a shoreline, defined as a land adjacent to the open bay or along a water pathway wider than 49 m. Oil within this 20 m zone will be referred to as shoreline oiling. The spatially contiguous and temporally persistent oiled marsh classes were primarily distributed along the shoreline (86.4% of pixels in these classes, covering 24.80 ha). Pixels in the lower probability oil class were also distributed along the shoreline but had a higher proportion of pixels in the marsh interior or along the edges of clouds (63.4% of pixels in this class).

3.7. Spatial characteristics of oiled zones

The vectorized oiled marsh map was used to calculate basic statistics for the linear extent of oiled marsh along the coast in north Barataria Bay. For the spatially contiguous and (or) temporally persistent classes, continuously oiled segments stretched on average 41.4 m along the coast (n = 654, std. dev. = 90.2 m, min = 3.5, max = 1099.0 m, median = 17.5 m). Excluding the Mud Lake area, the total length of oiled coastline, in the higher probability classes was 31.70 km. A total of 39.99 km of shoreline oiling was calculated by including shoreline pixels in the lower probability class.

Table 4
MICA spectral feature fit results for extracted AVIRIS pixel spectra.

Extracted AVIRIS pixel spectrum	MICA overall fit values to reference entries in the command file										
	Oiled-Plants3	Oiled-Plants2	Oiled-Plants1	Oiled-Marsh	Oiled-Dry Marsh	Oil-Strong	Veg-Dry Spartina	Veg-Dry Phragmites	Veg-Dry Spartina 2.3 μm only	Veg-Dry Phragmites 2.3 μm only	Veg-Strong Chlorophyll
Oiled-Plants2	0.8966	**0.9322**	0.9224	0.8970	0.9241	0.8599	0.8964	0.9219	0.8877	0.9252	0.0000
Oiled-Plants1	0.8665	0.8817	**0.8826**	0.8296	0.8558	0.8500	0.8088	0.8280	0.7671	0.8242	0.0000
Oiled-Marsh	0.9496	0.9599	0.9685	0.9760	**0.9858**	0.9372	0.8437	0.8775	0.8114	0.8757	0.0000
Oiled-Dry-Marsh	0.9023	0.9105	0.9299	0.9663	**0.9673**	0.9349	0.8502	0.8737	0.8097	0.8781	0.0000
Oil-Strong	0.9239	0.9383	0.9525	0.9314	0.9471	**0.9631**	0.8471	0.8871	0.8217	0.8867	0.0000
Veg-DrySpartina	0.7552	0.8113	0.7957	0.7138	0.7545	0.0000	0.8928	0.9119	**0.9876**	0.9791	0.0000
Veg-StrongChlorophyll	0.0000	0.0000	0.0000	0.0000	0.0000	0.0000	0.0000	0.0000	0.7839	0.7884	**0.9903**

Boldface indicates the best match (highest fit).

The penetration distance of the oil damage into the marsh in the Barataria Bay study area was evaluated by using the composite map and the higher-resolution data of that area collected on September 14 and October 4. In the composite map, the average penetration distance of shoreline oiling in the north Barataria Bay area was 11.0 m (n = 12,999; std. dev. = 4.7 m; median = 10.5 m). In the September 14 imagery, the average was 9.2 m (n = 5938; std. dev. = 3.9; median = 8.8). In the October 4 imagery, the average was 10.0 m (n = 6767; std. dev. = 3.6; median = 8.8). The maximum penetration distance, located in the Bay Jimmy subarea, was six pixels, equivalent to a maximum distance of penetration of 21 m.

3.8. Spatial and spectral resampling and mixture analysis

The impact of degrading the spatial resolution to 30 m GIFOV was assessed by aggregating the pixels of the 3.5 m AVIRIS data collected on October 4, 2010. An example of the MICA detection results for this coarser spatial resolution data in comparison to the original data is shown in Fig. 13. Generally, the larger concentrations of oiled marsh were still detected in the 30 m simulation. Overall accuracy using the coarser resolution data was 73.6%. An examination of the field verification points revealed that detection accuracy was high for points where oil damage extended more than 4 m into the marsh, 82.1% (23 of 28 oiled reference points), but low for less extensively oiled areas, 18.2% (2 of 11 oiled reference points).

An example of the results for the MESMA analysis of the simulated ETM data (Fig. 13C) is shown relative to the MICA analysis of the AVIRIS data (Fig. 13A) in which the central pixels of the oiled zones with deep penetration into the marsh were detected in the simulated ETM data but areas along the edges of these zones and oiling of relatively shallow penetration were missed. The MESMA analysis of the simulated ETM data at 30 m did not result in any detection of oiled marsh.

4. Discussion

The validation field spectra of oiled materials were matched to the reference spectra of the oiled materials without any confusion with the reference spectra of the non-oiled vegetation. Also with 100% accuracy, all 48 validation spectra of the non-oiled vegetation were matched to the reference spectra of the non-oiled vegetation. Testing of the MICA method with ten non-oiled, non-vegetation validation spectra resulted in no matches to either the reference spectra of the oiled materials or non-oiled vegetation. Considering that these non-oiled, non-vegetation validation spectra were measurements of water, dry and wet sand, and background marsh sediment, this result and the results presented in Table 5 for the validation spectra indicate that the MICA spectral feature comparison method is robust at identifying oiled and non-oiled vegetation, without confusion with other natural background materials.

In the maps of the oiled marsh derived from the AVIRIS data, the lack of open water pixels matched to the reference spectra of the oiled materials could indicate that other spectra need to be included in the reference spectra in order to detect oil in the open water areas (for example, see the oil emulsion spectra in Clark et al., 2010). Alternatively, oil emulsions were not present in the open water in sufficient abundance to be matched to one of the reference spectra, at the times the AVIRIS flights were conducted. Considering that the validation spectrum of oil-emulsion in water at the marsh edge was matched to a reference spectrum of pooled oil, any oil in the open water of Barataria Bay is likely to have been in the form of oil slicks and sheens, which do not show prominent C – H absorption features (see Clark et al., 2010).

At the remote sensing level, the MICA analysis of the AVIRIS reflectance data resulted in a very high level of accuracy in detecting oil-damaged marsh which extended more than 1.2 m of into the marsh. However, accuracy was lower for oil penetration ≤ 1.2 m. This detection limit applied to both the AVIRIS data with 7.6 m GIFOV collected in July and the 3.5 m GIFOV data collected in September and October. Defining the limit of detection based solely on the amount of pixels covered by the oiled marsh is complicated by the other factors that influence remotely sensed spectra. Each data collection had different atmospheric conditions and solar illumination and as a result the AVIRIS data in each date had varying degrees of residual, uncorrected atmospheric effects and uncorrected sun glint from the water's surface. Furthermore, the vegetation condition changed from the growing season to the onset of senescence, altering the vegetation contribution to each pixel's spectrum. The spectroscopic detection method was consistently successful in detecting oiled marsh in the individual dates despite these and additional complicating factors arising from fluctuating water levels causing variations in the amounts of background sediment or water below the canopy. These robust results demonstrate the applicability of spectroscopic remote sensing to rapid response situations when knowledge of contaminant distribution is needed for allocating resources for damage assessment, cleanup, and monitoring.

Beyond the detection of oil shown in this study, additional measures derived from spectral feature analysis, such as band depth or band area, could be examined for relation to the extent or amount of oiling in order to develop qualitative or quantitative measures of the fraction of oiled marsh in a pixel or, more broadly, oil abundance in a pixel. For example, band depths and band areas of continuum-removed features have been used to quantifying the biochemical content of vegetation (Kokaly & Clark, 1999; Kokaly et al., 2009).

As evidenced by the reference spectra of oil, oiled marsh, and background vegetation (see Fig. 2), the dry components of senescent or dead vegetation have spectral signatures that are similar to and overlap hydrocarbon absorption features. Along less-vegetated or non-vegetated coastlines, it is possible that lower limits of detection could be achievable as this overlapping absorption is reduced. Expanding the reference library by including mixtures of spectra of oiled vegetation and non-oiled vegetation to the reference spectral

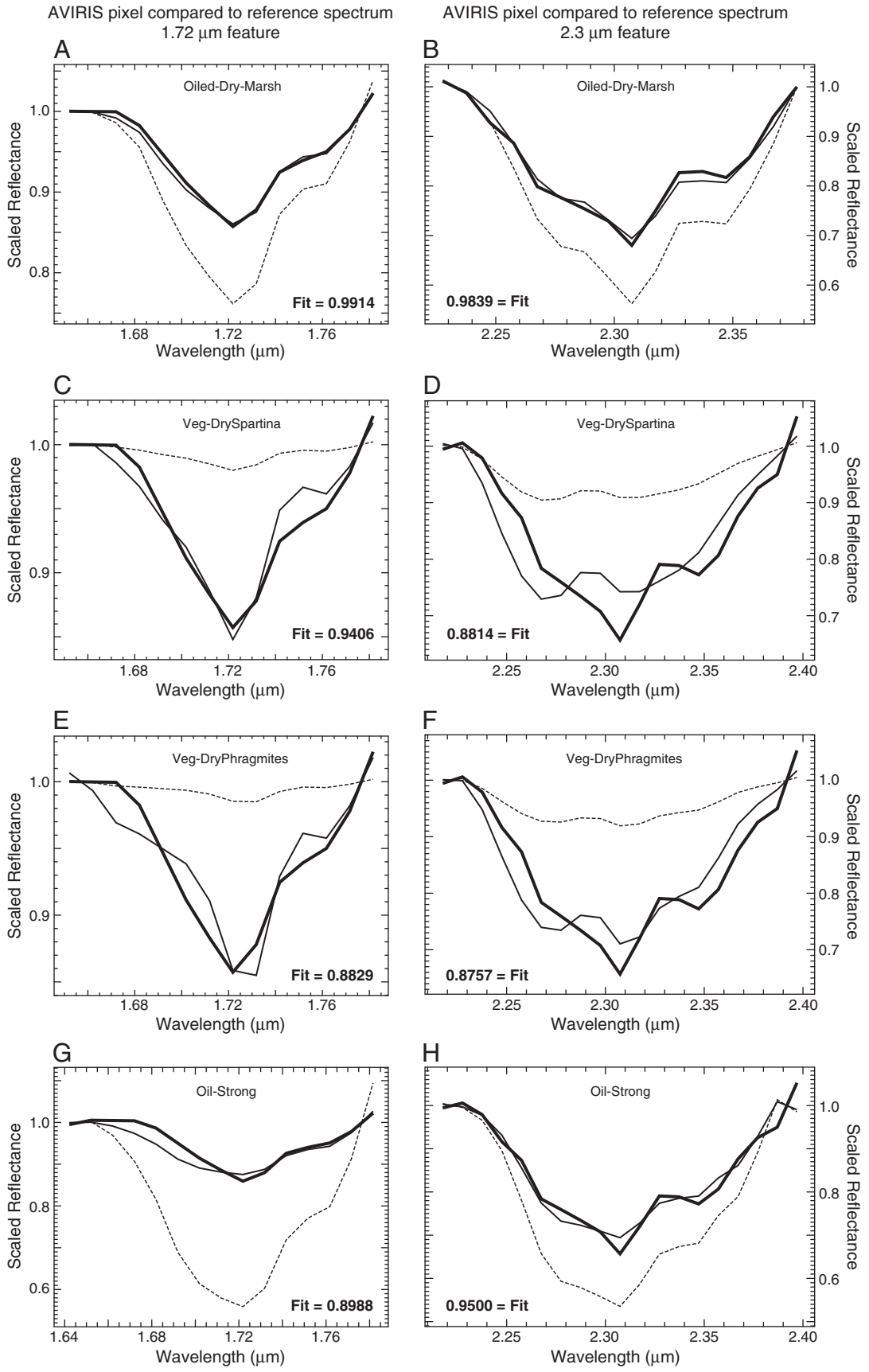
AVIRIS pixel compared to reference spectrum
1.72 μm feature
AVIRIS pixel compared to reference spectrum
2.3 μm feature
A
Oiled-Dry-Marsh
Fit = 0.9914
B
Oiled-Dry-Marsh
0.9839 = Fit
C
Veg-DrySpartina
Fit = 0.9406
D
Veg-DrySpartina
0.8814 = Fit
E
Veg-DryPhragmites
Fit = 0.8829
F
Veg-DryPhragmites
0.8757 = Fit
G
Oil-Strong
Fit = 0.8988
H
Oil-Strong
0.9500 = Fit
Scaled Reflectance
Wavelength (μm)

Table 5
MICA results for analysis of field validation spectra.

Material category	# of spectra	# matched to oiled reference spectra	# matched to non-oiled reference spectra	# not matched
Oiled materials	7	7	0	0
Non-oiled plants of single species	18	0	18	0
Non-oiled mixed plant material	2	0	2	0
Non-oiled plants of mixed species	28	0	28	0
Non-oiled, non-vegetation material	10	0	0	10

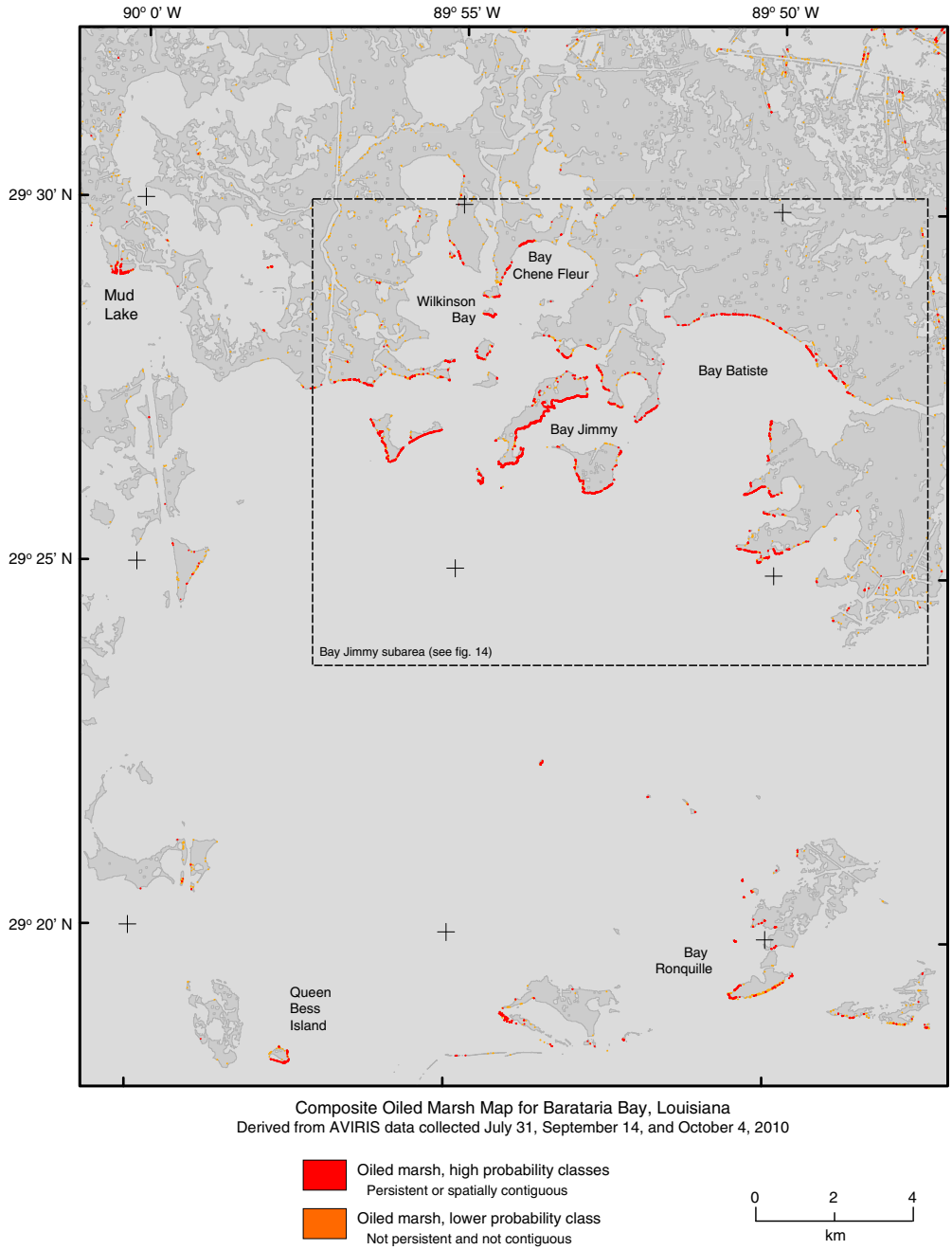

Fig. 11. Composite map of oiled marsh in Barataria Bay, Louisiana, derived from MICA analyses of AVIRIS data collected July 31, September 14, and October 4, 2010. Raster results were vectorized for depicting fine scale results over such a large area. The dashed-line box indicates the Bay Jimmy subarea. The raster-based results for this subarea are shown in Fig. 12. Depicted shorelines were derived from the AVIRIS data.

Fig. 10. Spectral feature comparison of an extracted AVIRIS pixel in the Oiled-Dry-Marsh reference location to reference spectra for: A) the 1.72 μm feature of the Oiled-Dry-Marsh reference spectrum, B) the 2.3 μm feature of the Oiled-Dry-Marsh reference spectrum, C) the 1.72 μm feature of the Veg-DrySpartina reference spectrum, D) the 2.3 μm feature of the Veg-DrySpartina reference spectrum, E) the 1.72 μm feature of the Veg-DryPhragmites reference spectrum, F) the 2.3 μm feature of the Veg-DryPhragmites reference spectrum, G) the 1.72 μm feature of the Oil-Strong reference spectrum, H) the 2.3 μm feature of the Oil-Strong reference spectrum. Red lines are the continuum-removed AVIRIS features, black, dashed lines are the continuum-removed reference features, and black, solid lines are the scaled reference features.

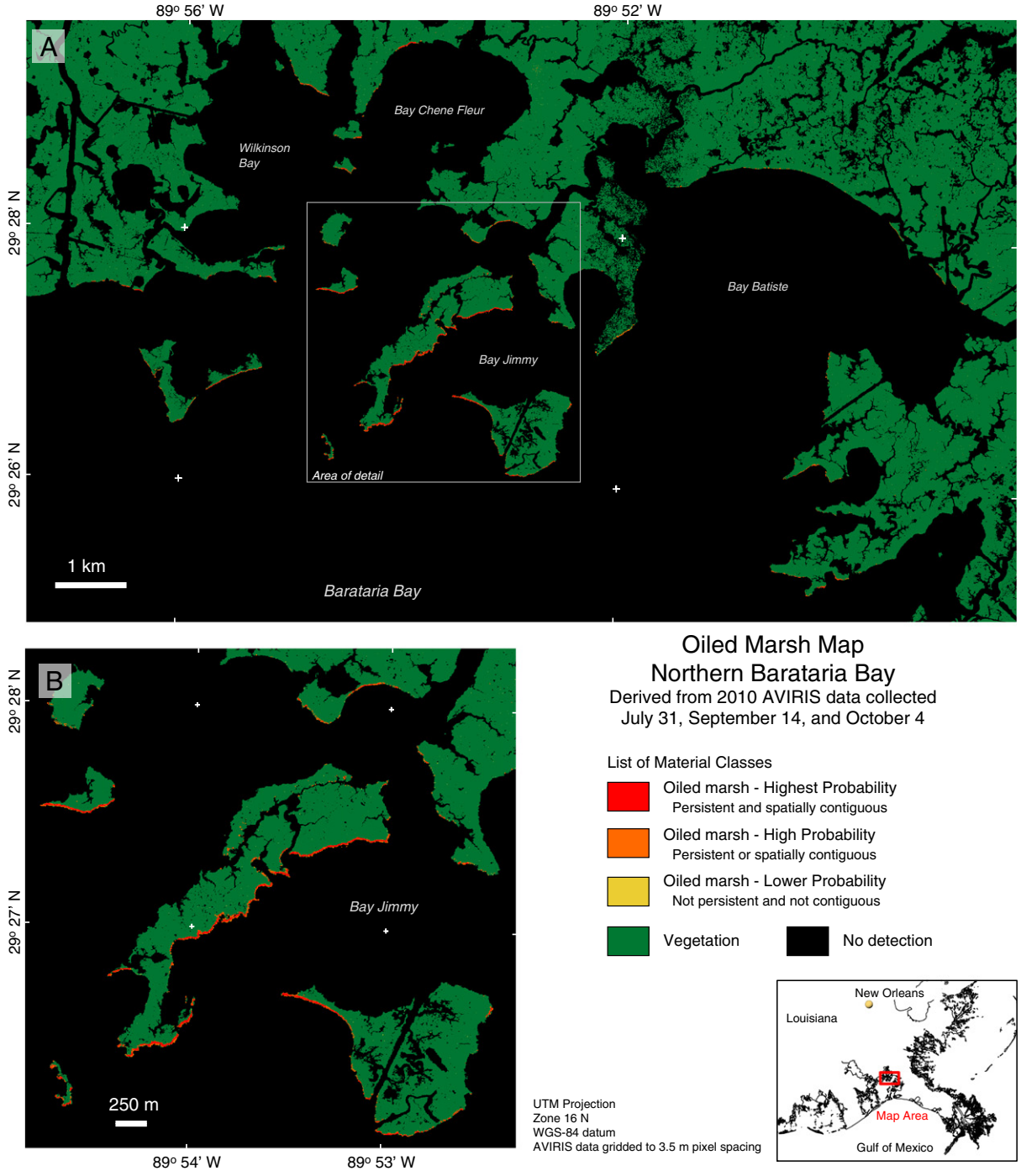

Fig. 12. A) Composite map of oiled marsh in the Bay Jimmy subarea derived from MICA analyses of AVIRIS data collected July 31, September 14, and October 4, 2010, and B) area of detail.

library might also lower the limit of detection. Achieving the best balance between lowering the limit of detection and avoiding false-positive detections should be studied in more detail.

The overlapping absorption caused by non-photosynthetic vegetation components, interfere with simple index calculations based on radiance data, such as the hydrocarbon index (HI; Kühn et al., 2004) targeted at the 1.72 μm C–H absorption feature.

$$HI = (\lambda_b - \lambda_a)/(\lambda_c - \lambda_a) * (R_c - R_a) + R_a - R_b \quad (1)$$

where λ_a = the wavelength position of a channel on the left side of the absorption feature, λ_b = the wavelength position of a channel at the center of absorption feature, and λ_c = the wavelength position of a channel on the right side of the absorption feature. R_a, R_b, and R_c refer to the radiance values in the channels at the λ_a, λ_b, and λ_c wavelength positions.

As a result of the overlap in oil-related C–H absorption and leaf biochemical absorption features in dry vegetation, it was expected that HI values of oiled marsh may not be reliably differentiated from high HI values in areas containing non-photosynthetic vegetation.

Table 6
Accuracy assessment of oiled marsh maps derived from AVIRIS data.

AVIRIS image date	Remote sensing class	Reference class (field observation)		User's accuracy	Overall accuracy
		Oil	Non-oil		
Composite	Oil	39	1	97.5%	93.4% (57 of 61)
	Non-oil	3	18	85.7%	
	Producer's accuracy	92.9%	94.7%		
July 31, 2010	Oil	33	1	97.1%	89.3% (50 of 56)
	Non-oil	5	17	77.3%	
	Producer's accuracy	86.8%	94.4%		
September 14, 2010	Oil	30	0	100.0%	89.8% (44 of 49)
	Non-oil	5	14	73.7%	
	Producer's accuracy	85.7%	100.0%		
October 4, 2010	Oil	34	1	97.1%	90.6% (48 of 53)
	Non-oil	4	14	77.8%	
	Producer's accuracy	89.5%	93.3%		

Following Kühn et al. (2004), but adapting channel selection to the AVIRIS sensor characteristics, we computed HI by using radiance data in the AVIRIS channels at 1.711, 1.731, and 1.741 μm. Fig. S3 in the Supplementary data shows the HI result in comparison to the MICA result for an area in Barataria Bay. Two color stretches were applied to the HI values. In the first stretch (Fig. S3b), color ranges were set to show HI values above 10 as red and orange colors. These high values appear along the shorelines in areas equivalent to the oiled marsh detections from the MICA method (Fig. S3a) but also along many other shorelines as well. In addition, considerable false positives were found in the interior marsh with the first color stretch. Adjusting the color stretch to show only HI values > 20 in red and orange colors (Fig. S3c), results in an image that fails to highlight the areas known to be oiled by the field survey (the field survey points are marked in Fig. S3) and fails to highlight the areas detected as oiled marsh in the MICA result.

The HI images derived from AVIRIS were, generally, very noisy in all three image dates. From Kühn et al. (2004): "The most accurate HI images are obtained for urban areas and bare ground, whereas areas that are largely covered by vegetation may appear 'noisy' in HI imagery. Dry vegetation can further limit the use of the HI. Dark-colored hydrocarbons are not detected reliably by the HI method." The spectra presented in Kühn et al. (2004) showed a well-defined absorption feature in the radiance spectra at the center wavelength of the HI channels (1.73 μm in radiance spectra). However, in most of the AVIRIS radiance spectra in this study only a slight inflection in the slope of the spectra was present, even in the confirmed areas of oiling. In addition, spikes in the AVIRIS data interfered with the use of HI, giving

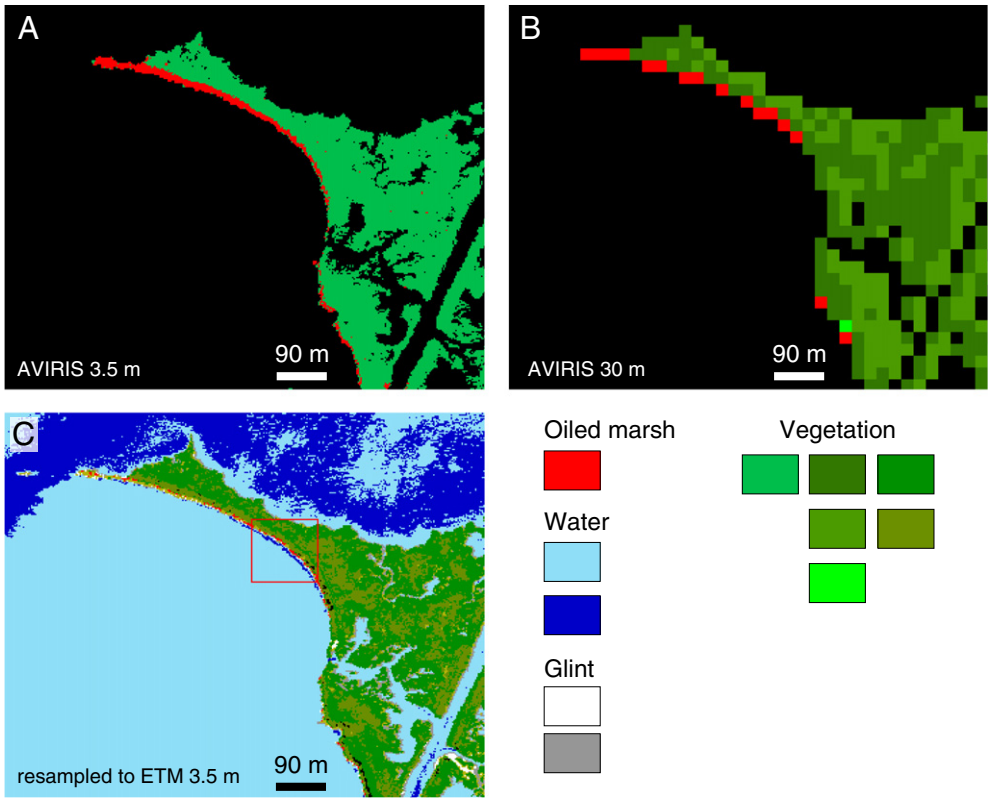

Fig. 13. Comparison images showing the impact of spatial and spectral resolutions on oil detection: A) MICA results for analysis of AVIRIS data at 3.5 m, B) MICA results for analysis of AVIRIS data at 30 m, and C) MESMA results for Landsat ETM simulation at 3.5 m.

false positives on the shoreline boundaries and, more generally, the edges of areas with a strong contrast in reflectance. The spectroscopic approach used in our study mitigated these problems by including senesced vegetation entries in the reference library and by using the 2.30 μm hydrocarbon absorption feature in addition to the 1.72 μm feature.

The results of spatial degradation of the AVIRIS data indicate that moderate spatial resolution imaging spectrometer data (30 m) collected from a satellite platform could detect subpixel occurrences of oiled marsh extending 4 m or greater from the shoreline, that is, oiled plants covering as little as 13% of a pixel. In this study, the pixel aggregation greatly increased the S/N compared to the S/N inherent in a single pixel of the original 3.5 m AVIRIS data. Thus, that level of detection is possible only if high signal:noise (S/N) reflectance data are available.

Discrimination of oiled marsh by using the AVIRIS data resampled to the Landsat ETM spectral responses was limited to the core areas of extensive oiling at 3.5 m GIFOV. Based on the lesser discriminating power of the multispectral data and narrow zones of oiling, it was expected that moderate and coarse resolution satellite sensors such as Landsat ETM and MODIS would be severely limited in their ability to directly detect oiled marsh. Indeed, the MESMA analysis for simulated 30 m ETM data was unable to detect oiled marsh. Landsat ETM spectra do not resolve the diagnostic C–H absorption features at 1.72 and 2.3 μm. Because of this lack of spectral leverage, the discrimination of oiled marsh impacts by using multispectral data will require the increased leverage supplied by time series analysis. By contrasting pre- and post-impact signatures, Mishra et al. (2012) showed differences in vegetation greenness trends in southern Louisiana by using Landsat data from 2009 to 2010. They inferred that these relative differences are a result of oil impact; however, multi-date comparisons add the confounding factors of seasonal and inter-annual changes, e.g., temperature, precipitation, and water salinity, that impede direct attribution of greenness changes to oil contamination. Because Mishra et al. (2012) used a field spectrometer that covered only a portion of the reflected solar range, they focused on changes in the chlorophyll feature in field reflectance data and NDVI (normalized difference vegetation index) in satellite data. By using imaging spectrometer data to resolve the C–H absorption features at 1.72 and 2.3 μm, our study was able to directly identify oil-damaged canopies in each single date of imagery.

Field observations revealed that oil damage to the marsh at some sites resulted in a complete reduction of live vegetation cover and erosion of exposed sediments, while other damaged zones had signs of regrowth of vegetation in up to 10% of the areal coverage by the end of August, 2010. In the field observations and oiled marsh maps, oil was found most frequently on the exposed south sides of land masses in Barataria Bay and less frequently on shores oriented in other directions and in protected coves. Oiled marsh detected on south-facing shorelines may be more vulnerable to erosion from storm-induced waves. In contrast, oil detected in the marsh interior and in protected coves and inlets may persist longer and might cause significant long-term damage due to less opportunity for natural flushing and human remediation.

The extent of the heavily oiled zones and the persistence of oil within the marshes indicate the potential for continued oil impact on vegetative regrowth within the zones of oil-damaged canopy and detrimental impacts on plant health in adjacent areas. The commonly occurring species at the shore of oiled zones of Barataria Bay, *S. alterniflora* and *J. roemerianus*, and less frequently occurring species, *S. patens*, *D. spicata*, and *P. australis*, have variable growth response in soils contaminated by fresh crude and fuel products (Lin & Mendelssohn, 1996, 2008, 2009). Past studies suggest that *S. alterniflora* might experience preferential growth in response to oiling, dependent on nutrient availability and species competition (Lin & Mendelssohn, 1998). The AVIRIS-based maps of oiling show the distribution of physically-damaged canopy and heavy oil deposition around which areas longer-term impacts may be examined.

Coastal Louisiana marshes have historically experienced high subsidence rates due to human disturbances of wetland habitat for purposes of flood protection, water supply, maritime commerce, and energy production; thus, organic matter production and mineral sedimentation are important in maintaining marsh elevation and sustainability (DeLaune et al., 2003; Kennish, 2001). If the initial dieback of above-ground vegetation in the oil-damaged canopy zones leads to successive decreases in below-ground biomass and/or stem densities that trap suspended sediments, the marsh may not be able to maintain sufficient elevation to prevent excessive inundation, and marsh loss could occur (DeLaune et al., 1994; Hartman, 1998; Nyman et al., 1993; Spalding & Hester, 2007; Turner et al., 2004). Conversely, if vegetation recolonization occurs quickly, the below-ground component should respond positively, and the marsh may maintain sufficient elevation to avoid loss. In this scenario, the oil spill may function as a temporary disturbance from which the marsh may quickly recover (Pezeshki et al., 2000).

A component of the dissolved fraction of organic carbon was anticipated to be derived through the degradation of hydrocarbons, potentially increasing the overall DOC concentrations. An incubation study of oil-contaminated surface waters from near the spill site found changes in fluorescence properties that suggest that oil-derived aromatic hydrocarbons were part of the DOC pool (Ziervogel et al., 2012). However, the DOC concentrations can also be affected by the biological uptake by microbial and vegetation communities. The DOC concentrations in water samples collected in this study are similar to the DOC concentrations previously reported for water samples collected from open water sites in the upper Barataria Bay ($n = 6$; 4.9–9.3 mg/L DOC) (Happ et al., 1977). Site DWO-4-BAT09 had visible oil sheen on the water and a greater DOC concentration (19.5 mg/L DOC) than other sites, possibly due to a recent influx of oil from open water through tidal or storm surge. The DOC data collected in 2010 suggest that either little of the crude oil distributed in marsh soils had been partitioned into the dissolved phase due to limited in situ biodegradation in the weeks following oiling may, or that DOC generated through the breakdown of crude oil in the marsh soils was rapidly taken up by growing vegetation and microbes. Emerging work on post-oiling marsh biogeochemistry (Natter, 2012) indicated that significant degradation of lighter weight petroleum compounds occurred, while heavier oils persisted in sediments. Thus, the DOC concentrations likely reflect a balance of rapid biological uptake of DOC and slow degradation rates of more recalcitrant petroleum residues.

In the Deepwater Horizon incident, oil was subject to weathering by evaporation, dissolution, oxidation and biodegradation before hitting the coast (Operational Science Advisory Team, 2010). Weathering has been shown to reduce the proportion of the more toxic, low molecular weight components of oil (Boesch et al., 1974; National Research Council Committee on Oil in the Sea, 2003). Sediments contaminated with oil which is lower in these components have been shown to result in lesser damage to plants (Cowell, 1969; Lin & Mendelssohn, 1998; Rosso et al., 2005). The range in depletion of low molecular weight composition in oil from the Deepwater Horizon incident along the coast (Operational Science Advisory Team, 2010) and our DOC concentration results indicate that the weathered oil on the coast of Barataria Bay may be causing less sustained chemical damage to adjacent areas than might have been experienced if fresh crude had hit the coast. However, there is a potential for sustained biogeochemical impact over time due to the large amount of oiling. During field surveys, consistent observations of oil sheen in waters of oiled areas were made over the course of several months. As the oil continues to degrade over time there is the potential to release DOC to marsh plants over multiple years. This increased carbon influx due to oiling could shift plant communities along the shoreline.

Additional collections of AVIRIS imaging spectrometer data covering Barataria Bay were completed in early May, July, and October,

2011. Those data, in conjunction with vegetation plot monitoring of species composition, cover, and biomass that we collected within a week of the airborne surveys, can be used to examine the continued persistence of surface oil in the marshes and degradation and recovery of vegetation in the areas of heavy oiling. The post-impact time series of AVIRIS data may also be applied to evaluating the efficacy of remediation and oil removal efforts and potentially applied to understanding other chemical impacts, such as from dispersants. Furthermore, these data will allow trends in marsh condition to be evaluated in adjacent areas, which may have been subject to partial oiling of stems or just inundation of oil sheens. Ramsey et al. (2011) analyzed UAVSAR backscatter data to classify areas of oil inundation. The radar results show the presence of oil sheens deeper in the marsh than the oil-damaged canopy detected using AVIRIS. The synthesis of the UAVSAR results with the 2010 AVIRIS maps of heavily oiled zones, and post-impact vegetation trends in 2011 AVIRIS may be useful for a full, longer-term understanding of the ecosystem response to oil contamination.

5. Conclusions

A spectroscopic approach to remote sensing was demonstrated to be a useful method for delineating oil contamination in marshes impacted during the Deepwater Horizon incident. Spectral feature analysis applied to the high spatial resolution (3.5 and 7.6 m) AVIRIS data were shown to be very accurate (93.4%) in detecting the hydrocarbon absorption features of oil and in mapping oiled marsh with a practical limit of detection of 1.2 m of oil penetration. In future applications, other airborne imaging spectrometers, with spatial GIFOV, spectral sampling and bandpass, and S/N characteristics similar to AVIRIS, should achieve comparable results to this study. Based on good accuracies in detecting oiled areas with physically damaged canopies that extended more than 4 m into the marsh using AVIRIS data degraded to 30 m, moderate resolution space borne imaging spectrometers with similar spectral characteristics and high S/N could be applied to detecting oiled shorelines. Because of the narrow zones of oil damage, on average 11 m, moderate and coarse resolution multispectral satellite sensors such as Landsat and MODIS will be severely limited in their ability to directly detect marsh oiled during the Deepwater Horizon incident.

At this point, it is difficult to predict the long term impact of a sudden dieback of large swaths of shoreline vegetation and the persistence of oil sources at the marsh edge. The maps derived from the 2010 collections of the AVIRIS data characterize the distribution and areal coverage of the oiled plant canopies and delineate the areas that experienced direct, physical damage to plant canopies. In these zones and adjacent areas, the deposited oil may continue to impact marsh plants. The degraded vegetation on the edge of the marsh increases the risk of land loss. Thus, these maps of oil contamination contribute to setting the context in which longer-term marsh degradation and recovery trends in response to oiling from the Deepwater Horizon incident can be understood.

Acknowledgments

Gregg Swayze and Greg Steyer of USGS assisted in field spectroscopy and design of field surveys, respectively. David Heckman (IAP Worldwide Services) and Kari Cretini (USGS) assisted with the vegetation identification. In response to the oil spill, the NASA AVIRIS team, including Robert Green, Michael Eastwood, Sarah Lundeen, Scott Nolte, and Charles Sarture, demonstrated outstanding service in the public interest. The Jet Propulsion Laboratory (JPL), Ellington Field, NASA Ames, Johnson Space Center and Dryden Flight Research Center supported the efforts to obtain airborne remote sensing data over oil-impacted areas of the coast. Dissolved organic carbon analysis was coordinated by George Aiken and Kenna Butler (USGS, Boulder, CO). The USGS field research was supported by the Pollution Removal Funding Authority and the Minerals and Health Project of the USGS Mineral Resources Program. The National Science Foundation provided funding to support this work (NSF RAPID grant #1058134 "Analysis of NASA's Advanced Visible Infrared Imaging Spectrometer data acquired over multiple dates and flightlines along the northern Gulf coastline, including barrier islands," Principal Investigator S. Ustin).

Disclaimer

Any use of trade, product, or firm names is for descriptive purposes only and does not imply endorsement by the U.S. Government.

Appendix A. Supplementary data

Supplementary data to this article can be found online at http://dx.doi.org/10.1016/j.rse.2012.10.028.

References

Aiken, G. R. (1992). Chloride interference in the analysis of dissolved organic carbon by the wet oxidation method. *Environmental Science and Technology*, *26*, 2435–2439.
Asner, G. P., & Vitousek, P. M. (2005). Remote analysis of biological invasion and biogeochemical change. *Proceedings of the National Academy of Sciences of the United States of America*, *102*, 4383–4386.
Boardman, J. (1999). Precision geocoding of low-altitude AVIRIS data: Lessons learned in 1998. *Summaries of the 8th JPL airborne earth science workshop, JPL Publication 99-17* (pp. 63–68).
Boesch, D. F., Hershner, C. H., & Milgram, J. H. (1974). *Oil spills and the marine environment* (pp. 21–23). Cambridge, MA: Ballinger.
Borja, A., Dauer, D. M., Elliot, M., & Simenstad, C. A. (2010). Medium- and long-term recovery of estuarine and coastal ecosystems: Patterns, rates and restoration effectiveness. *Estuaries and Coasts*, *33*, 1249–1260.
Carman, K. R., Fleeger, J. W., & Pomarico, S. M. (1997). Response of a benthic food web to hydrocarbon contamination. *Limnology and Oceanography*, *42*, 561–571.
Catallo, W. J. (1993). Ecotoxicology and wetland ecosystems: Current understanding and future needs. *Environmental Toxicology and Chemistry*, *12*, 2209–2224.
Chuang, W. S., & Wiseman, W. J., Jr. (1983). Coastal sea level response to frontal passages on the Louisiana–Texas shelf. *Journal of Geophysical Research*, *88*, 2615–2620.
Clark, R. N., & Roush, T. L. (1984). Reflectance spectroscopy: Quantitative analysis techniques for remote sensing applications. *Journal of Geophysical Research*, *89*, 6329–6340.
Clark, R. N., Swayze, G. A., Leifer, I., Livo, K. E., Kokaly, R., Hoefen, T., et al. (2010). A method for quantitative mapping of thick oil spills using imaging spectroscopy. *U.S. Geological Survey Open-File Report 2010-1167* (51 pp.).
Clark, R. N., Swayze, G. A., Livo, K. E., Kokaly, R. F., King, T. V. V., Dalton, J. B., et al. (2002). Surface reflectance calibration of terrestrial imaging spectroscopy data: A tutorial using AVIRIS. *Proceedings of the 10th airborne earth science workshop, JPL Publication 02-1*.
Clark, R. N., Swayze, G. A., Livo, K. E., Kokaly, R. F., Sutley, S. J., Dalton, J. B., et al. (2003). Imaging spectroscopy: Earth and planetary remote sensing with the USGS tetracorder and expert systems. *Journal of Geophysical Research*, *108*, 5131–5146.
Clark, R. N., Swayze, G. A., Wise, R., Livo, E., Hoefen, T., Kokaly, R., et al. (2007). *USGS digital spectral library splib06a.* U.S. geological survey digital data series 231. http://speclab.cr.usgs.gov/spectral.lib06
Cloutis, E. A. (1989). Spectral reflectance properties of hydrocarbons: Remote-sensing implications. *Science*, *245*, 165–168.
Congalton, R. G., & Mead, R. A. (1983). A quantitative method to test for consistency and correctness in photointerpretation. *Photogrammetric Engineering and Remote Sensing*, *49*, 69–74.
Couvillion, B. R., Barras, J. A., Steyer, G. D., Sleavin, W., Fischer, M., & Beck, H., et al. (2011). Land area change in coastal Louisiana from 1932 to 2010, U.S. Geological Survey Scientific Investigations Map 3164, scale 1:265,000, 12 pp.
Cowell, E. B. (1969). The effects of oil pollution on salt–marsh communities in Pembrokeshire and Cornwall. *Journal of Applied Ecology*, *6*, 133–142.
Crone, T. J., & Tolstoy, M. (2010). Magnitude of the 2010 Gulf of Mexico oil leak. *Science*, *330*, 634.
Day, J. W., Jr., Barras, J., Clairain, E., Johnston, J., Justic, D., Kemp, G. P., et al. (2005). Implications of global climatic change and energy cost and availability for the restoration of the Mississippi Delta. *Ecological Engineering*, *24*, 253–265.
DeLaune, R. D., Jugsujinda, A., Peterson, G. W., & Patrick, W. H., Jr. (2003). Impact of Mississippi River freshwater reintroduction on enhancing marsh accretionary processes in a Louisiana estuary. *Estuarine, Coastal and Shelf Science*, *58*, 653–662.
DeLaune, R. D., Nyman, J. A., & Patrick, W. H., Jr. (1994). Peat collapse, ponding and wetland loss in a rapidly submerging coastal marsh. *Journal of Coastal Research*, *10*, 1021–1030.
Dennison, P. E., Charoensiri, K., Roberts, D. A., Peterson, S. H., & Green, R. O. (2006). Wildfire temperature and land cover modeling using hyperspectral data. *Remote Sensing of Environment*, *100*, 212–222.
Dennison, P. E., & Roberts, D. A. (2003). Endmember selection for multiple endmember spectral mixture analysis using endmember average RSME. *Remote Sensing of Environment*, *87*, 123–135.

Elvidge, C. D. (1990). Visible and near infrared reflectance characteristics of dry plant materials. *Remote Sensing of Environment*, *11*, 1775–1795.
Green, R. O., Eastwood, M. L., Sarture, C. M., Chrien, T. G., Aronsson, M., Chippendale, B. J., et al. (1998). Imaging spectroscopy and the airborne visible/infrared imaging spectrometer (AVIRIS). *Remote Sensing of Environment*, *65*, 227–248.
Happ, G., Gosselink, J. G., & Day, J. W., Jr. (1977). The seasonal distribution of organic carbon in a Louisiana estuary. *Estuarine and Coastal Marine Science*, *5*, 695–705.
Hartman, J. M. (1998). Recolonization of small disturbance patches in a New England salt marsh. *American Journal of Botany*, *75*, 1625–1631.
Kennish, M. J. (2001). Coastal salt marsh systems in the U.S. A review of anthropogenic impacts. *Journal of Coastal Research*, *17*, 731–748.
Ko, J. Y., & Day, J. W. (2004). A review of ecological impacts of oil and gas development on coastal ecosystems in the Mississippi Delta. *Ocean and Coastal Management*, *47*, 597–623.
Kokaly, R. F. (2011). PRISM: Processing routines in IDL for spectroscopic measurements (installation manual and user's guide, version 1.0). *U.S. geological survey open-file report 2011-1155* (432 pp., available at http://pubs.usgs.gov/of/2011/1155/.)
Kokaly, R. F., Asner, G. P., Ollinger, S. V., Martin, M. E., & Wessman, C. A. (2009). Characterizing canopy biochemistry from imaging spectroscopy and its application to ecosystem studies. *Remote Sensing of Environment*, *113*, S78–S91.
Kokaly, R. F., & Clark, R. N. (1999). Spectroscopic determination of leaf biochemistry using band-depth analysis of absorption features and stepwise multiple linear regression. *Remote Sensing of Environment*, *67*, 267–287.
Kokaly, R. F., Despain, D. G., Clark, R. N., & Livo, K. E. (2003). Mapping vegetation in Yellowstone National Park using spectral feature analysis of AVIRIS data. *Remote Sensing of Environment*, *84*, 437–456.
Kokaly, R. F., Despain, D. G., Clark, R. N., & Livo, K. E. (2007b). Spectral analysis of absorption features for mapping vegetation cover and microbial communities in Yellowstone National Park using AVIRIS data. In L. A. Morgan (Ed.), *Chapter N of integrated geoscience studies in the Greater Yellowstone area — Volcanic, tectonic, and hydrothermal processes in the Yellowstone geoecosystem. U.S. geological survey professional paper 1717* (26 pp.).
Kokaly, R. F., Heckman, D., Holloway, J., Piazza, S., Couvillion, B., Steyer, G. D., et al. (2011). Shoreline surveys of oil-impacted marsh in southern Louisiana, July to August 2010. *U.S. geological survey open-file report 2011-1022* 124 pp., available at http://pubs.usgs.gov/of/2011/1022/.
Kokaly, R. F., Hoefen, T. M., Livo, K. E., Swayze, G. A., Leifer, I., McCubbin, I. B., et al. (2010). A rapid method for creating qualitative images indicative of thick oil emulsion on the ocean's surface from imaging spectrometer data. *U.S. geological survey open-file report 2010-1107* (16 pp.).
Kokaly, R. F., Rockwell, B. W., Haire, S. L., & King, T. V. V. (2007). Characterization of post-fire surface cover, soils, and burn severity at the Cerro Grande Fire, New Mexico, using hyperspectral and multispectral remote sensing. *Remote Sensing of Environment*, *106*, 305–325.
Kühn, F., Oppermann, K., & Hörig, B. (2004). Hydrocarbon Index — An algorithm for hyperspectral detection of hydrocarbons. *International Journal of Remote Sensing*, *22*, 1413–1422.
Lammoglia, T., & Souza Filho, C. R. (2011). Spectroscopic characterization of oils yielded from Brazilian offshore basins: Potential applications of remote sensing. *Remote Sensing of Environment*, *115*, 2525–2535.
Lammoglia, T., & Souza Filho, C. R. (2012). Mapping and characterization of the API gravity of offshore hydrocarbon seepages using multispectral ASTER data. *Remote Sensing of Environment*, *123*, 381–389.
Li, L., Ustin, S. L., & Lay, M. (2005). Application of AVIRIS data in detection of oil-induced vegetation stress and cover change at Jornada, New Mexico. *Remote Sensing of Environment*, *94*, 1–16.
Lin, Q., & Mendelssohn, I. A. (1996). A comparative investigation of the effects of Louisiana crude oil on the vegetation of fresh, brackish, and salt marsh. *Marine Pollution Bulletin*, *32*, 202–209.
Lin, Q., & Mendelssohn, I. A. (1998). The combined effects of phytoremediation and biostimulation in enhancing habitat restoration and oil degradation of petroleum contaminated wetlands. *Ecological Engineering*, *10*, 263–274.
Lin, Q., & Mendelssohn, I. A. (2008). Determining tolerance limits for restoration and phytoremediation with *Spartina patens* in crude oil-contaminated sediment in greenhouse. *Archives of Agronomy and Soil Science*, *54*, 681–690.
Lin, Q., & Mendelssohn, I. A. (2009). Potential of restoration and phytoremediation with *Juncus roemerianus* for diesel-contaminated coastal wetlands. *Ecological Engineering*, *35*, 85–91.
Louisiana Office of Coastal Protection and Restoration (2012). *Coastwide reference monitoring system — Wetlands monitoring data.* Retrieved from Strategic Online Natural Resource Information System (SONRIS) database (http://dnr.louisiana.gov/crm/coastres/monitoring.asp Accessed August 2, 2012.)
Mishra, D. R., Cho, H. J., Ghosh, S., Fox, A., Downs, C., Merani, P. B. T., et al. (2012). Post-spill state of the marsh: Remote estimation of the ecological impact of the Gulf of Mexico oil spill on Louisiana salt marshes. *Remote Sensing of Environment*, *118*, 176–185.
National Committee on the BP Deepwater Horizon Oil Spill and Offshore Drilling (2011). *Deep water: The Gulf Oil disaster and the future of offshore drilling.* Report to the President.
National Research Council Committee on Oil in the Sea (2003). *Oil in the Sea III: Inputs, fates, and effects.* Washington, D.C.: National Academies Press.
Natter, M. G. (2012) Fate and transformations of oils and trace metals in Alabama and Louisiana coastal marsh sediments associated with the British Petroleum Gulf oil spill. M.S. Thesis, Auburn University, Auburn, AL, 169 pp.
Nyman, J. A., DeLaune, R. D., Roberts, H. H., & Patrick, W. H., Jr. (1993). Relationship between vegetation and soil formation in a rapidly submerging coastal marsh. *Marine Ecology Progress Series*, *96*, 269–279.
Operational Science Advisory Team (2010). *Summary report for sub-sea and sub-surface oil and dispersant detection: Sampling and monitoring.* Prepared for U.S. Coast Guard Federal On-Scene Coordinator Deepwater Horizon MC252.
Pezeshki, S. R., Hester, M. W., Lin, Q., & Nyman, J. A. (2000). The effect of oil spill and cleanup on dominant US Gulf coast marsh macrophytes: A review. *Environmental Pollution*, *180*, 129–139.
Ramsey, E., III, Rangoonwala, A., Suzuoki, Y., & Jones, C. E. (2011). Oil detection in a coastal marsh with polarimetric synthetic aperture radar (SAR). *Remote Sensing*, *3*, 2630–2662.
Riaño, D., Chuvieco, E., Ustin, S. L., Zomer, R., Dennison, P., Roberts, D., et al. (2002). Assessment of vegetation regeneration after fire through multitemporal analysis of AVIRIS images in the Santa Monica Mountains. *Remote Sensing of Environment*, *79*, 60–71.
Roberts, D. A., Gardner, M., Church, R., Ustin, S., Scheer, G., & Green, R. O. (1998). Mapping chaparral in the Santa Monica Mountains using multiple endmember spectral mixture models. *Remote Sensing of Environment*, *65*, 267–279.
Rosso, P. H., Pushnik, J. C., Lay, M., & Ustin, S. L. (2005). Reflectance properties and physiological responses of *Salicornia virginica* to heavy metal and petroleum contamination. *Environmental Pollution*, *137*, 241–252.
Sasser, C. E., Visser, J. M., Mouton, E., Linscombe, J., & Hartley, S. B. (2008). Vegetation types in coastal Louisiana in 2007: U.S. geological survey open-file report 2008–1224, 1 sheet, scale 1:550,000.
Shoreline Cleanup Assessment Techniques (SCAT) maps (2012). Available at http://gomex.erma.noaa.gov/erma.html
Snedden, G. 2006. River, tidal, and wind interactions in a deltaic estuarine system. PhD Dissertation, Louisiana State University. 104 pp.
Spalding, E. A., & Hester, M. W. (2007). Interactive effects of hydrology and salinity on oligohaline plant species productivity: Implications of relative sea-level rise. *Estuaries and Coasts*, *30*, 214–225.
Steyer, G. D., Sasser, C. E., Visser, J. M., Swensen, E. M., Nyman, J. A., & Raynie, R. C. (2003). A proposed coast-wide reference monitoring system for evaluating wetland restoration trajectories in Louisiana. *Environmental Monitoring and Assessment*, *81*, 107–117.
Tanré, D., Deschamps, P. Y., Duhaut, P., & Heman, M. (1987). Adjacency effect produced by the atmospheric scattering in thematic mapper data. *Journal of Geophysical Research*, *92*, 12000–12006.
Turner, R. E., Swenson, E. M., Milan, C. S., Lee, J. E., & Oswald, T. A. (2004). Below-ground biomass in healthy and impaired salt marshes. *Ecological Research*, *19*, 29–35.
Ziervogel, K., McKay, L., Rhodes, B., Osburn, C. L., Dickson-Brown, J., Arnosti, C., et al. (2012). Microbial activities and dissolved organic matter dynamics in oil-contaminated surface seawater from the Deepwater Horizon oil spill site. *PLoS One*, *7*(4), e34816. http://dx.doi.org/10.1371/journal.pone.0034816.